1 **Title**

2 A novel role for *Ets4* in axis specification and cell migration in the spider

3 *Parasteatoda tepidariorum*

4

5 **Authors/Affiliations**

6 Matthias Pechmann[1*], Matthew A. Benton[1], Nathan J. Kenny[2], Nico Posnien[3],

7 Siegfried Roth[1]

8

9 [1]Institute for Developmental Biology, University of Cologne, 50674 Cologne, North-

10 Rhine Westphalia, Germany

11 [2]Life Sciences Department, The Natural History Museum, Cromwell Road, London

12 SW7 5BD, UK

13 [3]Department of Developmental Biology, GZMB, University Göttingen, 37077

14 Göttingen, Lower Saxony, Germany

15

16 **Corresponding Author**

17 * Matthias Pechmann (M.P.)

18 pechmanm@uni-koeln.de

19

20 **Keywords**

21 *Ets4/Ets98B*, spider, *Parasteatoda tepidariorum*, cumulus, cell migration,

22 dorsoventral, axis formation, organizer

23

24

25

26

Abstract

Organizers play important roles during the embryonic development of many animals. The most famous example is the Spemann organizer that sets up embryonic axes in amphibian embryos.

In spiders, a group of BMP secreting mesenchymal cells (the cumulus) functions as an organizer of the dorsoventral axis. Similar to experiments performed with the Spemann organizer, transplantation of the cumulus is able to induce a secondary axis in spiders.

Despite the importance of this structure, it is unknown which factors are needed to activate cumulus specific gene expression.

To address this question, we performed a transcriptomic analysis of early embryonic development in the spider *Parasteatoda tepidariorum.* Through this work, we found that the transcription factor *Pt-Ets4* is needed for cumulus integrity, dorsoventral patterning and for the activation of *Pt-hunchback* and *Pt-twist* expression. Furthermore, ectopic expression of *Pt-Ets4* is sufficient to induce cell delamination and migration by inducing a mesoderm-like cell fate.

Introduction

The self-regulatory capacities of vertebrate embryos were most famously demonstrated by Spemann and Mangold. They found that by grafting the dorsal-lip of an amphibian embryo (now known as the Spemann Organizer) to the ventral side of the host gastrula embryo it was possible to induce a secondary body axis [1-3].

Intriguingly, also spider embryos have high self-regulatory capacities, even to the extent that twinning can occur spontaneously [4]. During spider embryogenesis a group of migratory cells (the cumulus) is needed to break the radial symmetry of the early embryo and to induce the dorsoventral body axis [4-10]. Similar to the

vertebrate experiments, Holm showed that transplanting cumulus material was able to induce a secondary axis in spider embryos [11]. Modern work has shown that the cumulus signals via BMP signaling (again, similar to vertebrates). The mesenchymal cumulus cells are the source of the BMP receptor ligand Decapentaplegic [6]. Interfering with the BMP signaling pathway by gene knockdown results in the loss of dorsal tissue identity, which in turn leads to completely radially-symmetric and ventralized embryos [6]. The cumulus forms in the center of the so-called germ-disc (the embryonic pole of the embryo) and migrates underneath the ectoderm towards the rim of the disc. Arrival of the cumulus at the rim induces the opening of the germ-disc [4-10]. Cumulus migration is dependent on the Hh-signaling pathway [12] and it was shown that the knockdown of components of this signaling pathway results in cumulus migration defects and in the ectopic opening of the germ-disc [12].

How the cumulus is specified and forms is still under debate. During the formation of the germ-disc a small cluster of cells gastrulate and form an indentation where the future center of the fully formed germ-disc will be located. This cluster of cells appears as a visible spot and is called the primary thickening [5, 8]. However it is not clear whether all or only a subset of the cells of the primary thickening give rise to the cumulus, or if cumulus cells arise from subsequent cell invagination at the site of the primary thickening [4, 5]. Cell tracing [11, 13], as well as the expression of the endodermal marker *forkhead* [14] within the primary thickening/cumulus cells led to the suggestion that the primary thickening/cumulus cells are central endodermal cells [8, 14]. However, these studies could not completely rule out that the labeled cumulus cells develop into cells of the visceral mesoderm [13].

During the last 15 years, research focused on candidate genes known to be involved in development in *Drosophila melanogaster* has revealed several aspects of how spider embryos pattern their main body axis. However, there are many open

79 questions regarding the early regulation of cumulus specific gene expression,
80 cumulus establishment and maintenance.

81 To overcome the limitations of the candidate gene approach, we have carried
82 out transcriptome sequencing of carefully staged embryos to find new genes involved
83 in cumulus and axial patterning in the spider *Parasteatoda tepidariorum*. From this
84 work, we have identified the transcription factor Pt-Ets4 as a new gene expressed
85 during early development and have found it to be expressed exclusively within the
86 central primary thickening and the cells of the migrating cumulus. Our combined
87 genetic and cellular analyses show that Pt-Ets4 is needed for the integrity of the
88 cumulus. We found that the knockdown of this gene leads to embryos that show axis
89 patterning defects reminiscent to BMP knockdown phenotypes, suggesting that an
90 intact cumulus is needed to induce the formation of the bilaterally symmetric spider
91 embryo. Importantly, Pt-Ets4 is necessary and sufficient for driving the early
92 expression of *twist* (a gene involved in gastrulation and mesoderm formation in
93 *Drosophila*) and *hunchback,* and the ectopic expression of Pt-Ets4 is sufficient to
94 induce cell delamination.
95
96 **Results**
97 The formation of the germ-disc is one of the most important events during spider
98 embryogenesis. While a regular blastoderm (with no visible axial polarity) is present
99 at stage 2, the germ-disc condenses during stage 3 of embryonic development
100 (Figure 1A and B, for detailed description see [15]). This event leads to the
101 establishment of the anterior/posterior body axis (anterior: rim of the disc; posterior:
102 center of the disc).

103 To find new genes that are involved in the process of axis specification we
104 sequenced the embryonic transcriptomes of stage 1, stage 2 and stage 3 embryos

(Figure 1—figure supplement 1) and searched for genes showing a similar expression profile as *Pt-decapentaplegic* (*Pt-dpp), Pt-hedgehog* (*Pt-hh*) and *Pt-patched* (*Pt-ptc*) (representing genes that show early transcription and are required for axis formation or cumulus migration, respectively [6, 12]; Figure 1—figure supplement 1). One of the candidates was an *Ets*-like gene with high similarity to *Drosophila melanogaster Ets4/Ets98B* (see Figure 1—figure supplement 2), henceforth called *Parasteatoda tepidariorum Ets4* (*Pt-Ets4*).

Pt-Ets4 is expressed in the migrating cumulus

Prior to germ-disc condensation, *Pt-Ets4* is expressed within the cluster of cells that will form the center of the future germ-disc at early stage 3 (Figure 1A). Expression persists throughout germ-disc formation and, at stage 4, *Pt-Ets4* is strongly and exclusively expressed within the central cluster of cells (the so-called primary thickening, Figure 1B) that has delaminated during germ-disc formation (Figure 1C). During stage 5, the cumulus starts to migrate from the center of the germ-disc to its periphery [4-10]. At this stage *Pt-Ets4* is strongly and exclusively expressed in the migrating cumulus cells (Figure 1D and D').

We were not able to detect *Pt-Ets4* transcripts in ovaries and early stage 1 embryos via RNA *in situ* hybridization (Figure 1—figure supplement 3A and B). In addition, our sequencing data shows that *Pt-Ets4* is only expressed at a very low level during early stage 1, but is mildly up-regulated at late stage 2 and strongly up-regulated at early stage 3 (Figure 1—figure supplement 1). From this we conclude that *Pt-Ets4* transcripts are not maternally provided.

Pt-Ets4 is necessary for the integrity of the cumulus

Time-lapse imaging and cross-sectioning revealed that the knockdown of *Pt-Ets4* neither affected formation of the germ-disc nor of the primary thickening/cumulus (Video 1B; middle column in Figure 2, Figure 3A and B). However, during stage 5, cumulus integrity was affected in *Pt-Ets4* knockdown embryos (Video 1B, middle column in Figure 2). While in control embryos the cumulus migrated towards the rim (Video 1A, left column in Figure 2), the cumulus of *Pt-Ets4* RNAi embryos remained at the center of the germ-disc until early stage 5 and disappeared soon after gastrulation was initiated at the center and at the rim of the disc (Video 1B (15h onwards), middle column in Figure 2). Analysis of mid-stage 5 *Pt-Ets4* RNAi embryos for the expression of the cumulus marker *Pt-fascin* [12] revealed that although the cells of the cumulus were still in the center of the germ-disc, they appeared to be more loosely organized (Figure 3C and D).

In *Pt-Ets4* knockdown embryos the radial symmetry of the germ-disc was not broken (as shown by the formation of a tube-like germ band in Video 1B (30h onwards), and the middle column in Figure 2), presumably due to the loss of the cumulus. To investigate this phenotype in more detail, we knocked down another gene that also results in defects in radial symmetry breaking, *Pt-ptc*. In *Pt-ptc* knockdown embryos, cumulus migration is lost but the cumulus itself is otherwise unaffected [12]. After pRNAi with *Pt-ptc,* the cumulus stays in the center of the germ-disc (Video 1C; right column in Figure 2) and BMP signaling is ectopically activated (as shown via antibody staining against the phosphorylated form of mothers against dpp (pMAD) [12]. As a result, the germ-disc ectopically opened at the center and the dorsal field was induced at the posterior pole of the *Pt-ptc* RNAi embryos (right column in Figure 2). This ectopic induction of the dorsal field in the center of the germ-disc was never observed in the *Pt-Ets4* RNAi embryos. To test if the

disappearing cumulus was at least partially able to activate BMP signaling in the germ-disc of *Pt-Ets4* RNAi embryos, we performed a pMAD antibody staining in both control and *Pt-Ets4* RNAi embryos. In control embryos the cumulus reached the periphery of the germ-disc at late stage 5 and a strong pMAD staining was visible in the overlying ectodermal cells (Figure 3E, Figure 3—figure supplement 1). At this stage, the anterior marker *Pt-orthodenticle* (*Pt-otd*) was expressed in a ring, which had a width of 3-5 cells [5, 16, 17] (Figure 3E). In *Pt-Ets4* knockdown embryos *Pt-otd* expression was unaffected but nuclear pMAD was not detectable (Figure 3F). This lack of BMP signaling explains why *Pt-Ets4* RNAi embryos do not induce the dorsal field and stay radially symmetric. Indeed, the knockdown embryos were completely ventralized; the expression of the ventral marker *Pt-short-gastrulation* (*Pt-sog*) was uniform around the embryonic circumference and the segmental marker *Pt-engrailed* (*Pt-en*) was expressed in symmetric rings demonstrating the radial symmetry of the embryo (Figure 3G-L). During later development the embryonic tissue either grew completely over the yolk (Figure 3J-L), or a tube like structure elongated at the posterior of the embryo (Video 1B, middle column Figure 2). This was in contrast to *Pt-ptc* RNAi embryos, where the germ-disc opened up centrally and a tube like structure formed at the anterior of the embryo (right column Figure 2; Video 1C).

The *Pt-Ets4* knockdown phenotype is rather similar to that of *Pt-dpp*, although cumulus migration/integrity is not affected in *Pt-dpp* RNAi embryos [6]. This observation, plus the early and strong expression of *Pt-Ets4* and the fact that BMP signaling disappeared upon *Pt-Ets4* knockdown, led us to hypothesize that *Pt-Ets4* functions as an activator of *Pt-dpp* transcription within the cells of the cumulus. However, there was no obvious difference in the expression of *Pt-dpp* in stage 4 control and *Pt-Ets4* RNAi embryos (Figure 4A and E). Vice versa, *Pt-dpp* appears not to be regulating the expression of *Pt-Ets4* (Figure 4—figure supplement 1A). In

addition, Hh signaling seems not to be involved in the regulation of *Pt-Ets4* expression and *Pt-Ets4* appears not to regulate the expression of *Pt-ptc* within the primary thickening (Figure 4—figure supplement 1B and C).

In order to determine what other genes *Pt-Ets4* may regulate, we studied the expression of genes normally expressed in the primary thickening in *Pt-Ets4* RNAi embryos. We found that *Pt-forkhead* (*Pt-fkh*) expression was unaffected (Figure 4B and F), while the cumulus marker *Pt-fascin* was slightly down regulated, and *Pt-hunchback* (*Pt-hb*) was strongly down regulated in *Pt-Ets4* knockdown embryos (Figure 4C, D, G and H).

Ectopic expression of *Pt-Ets4* induces cell migration

As *Pt-Ets4* is strongly expressed in the cumulus and is required for cumulus integrity, we wondered how ectopic expression of *Pt-Ets4* would affect cell behavior. To generate small cell clones ectopically expressing Pt-Ets4 within the germ-disc, we micro-injected late stage 1 embryos (via single cell/blastomere injections [8, 18]) with *in vitro* synthesized capped mRNA coding for an EGFP-Pt-Ets4 fusion protein (see Figure 5—figure supplement 1).

Our first observation was that the EGFP-Pt-Ets4 fusion protein localizes to the nuclei of the injected cells, suggesting that the nuclear-localization-signal of Pt-Ets4 is functioning normally (Figure 5A). EGFP-Pt-Ets4 marked cell clones resembled wild-type until stage 4. As soon as a dense germ-disc formed, however, the cell clones expressing EGFP-Pt-Ets4 seemed to move beneath the germ-disc and the EGFP signal became occluded by the opaque cells of the germ-disc (Figure 5B). We have never seen such behavior following injection of EGFP-NLS constructs alone (Figure 5F-F'''), indicating that the change in cell behavior is due to the ectopic expression of *Pt-Ets4*.

To further visualize the process of cell clone delamination, we marked cell membranes by co-injecting capped mRNA coding for EGFP-Pt-Ets4 together with capped mRNA coding for lynGFP [19]. In control embryos (ectopic expression of lynGFP alone), lynGFP strongly marked the cell outlines of control embryos and cell clones stayed at the surface epithelium of the germ-disc (Video 2A, Figure 5C-C''). Regardless of the position and the shape of the cell clone, cells expressing lynGFP/EGFP-Pt-Ets4 constricted and delaminated shortly after the formation of the germ-disc (Video 2B-D, Figure 5D-D''). The detection of EGFP-Pt-Ets4 cell clones in fixed embryos using an antibody against EGFP confirmed that the labeled cells were below the epithelium of the germ-disc (Figure 5E and E').

The nuclear signal of the EGFP-Pt-Ets4 fusion construct (and the membrane signal of the lynGFP) is hardly visible after the delamination process. Therefore, we co-injected capped mRNA for EGFP-Pt-Ets4 with capped mRNA for nuclear localized EGFP (EGFP-NLS, see Figure 5—figure supplement 1), a construct that we have found to produce a very bright and persistent fluorescent signal. This experiment resulted in a strong nuclear localized EGFP signal within the marked cell clone, which we used to perform time-lapse imaging. While in the control embryos (injected with EGFP-NLS alone) the marked cell clones persisted at the surface of the germ-disc (Video 3A, Figure 5F and F'), the cell clone expressing both EGFP-NLS and EGFP-Pt-Ets4 delaminated shortly after the formation of the germ-disc (Video 3B, Figure 5G and G'). As previously shown [18, 20], germ-disc cells continue to divide and undergo convergent extension during the formation of the germ-band, which causes cell clones to become thin and elongated as seen in our control EGFP-NLS clones (Video 3A, Figure 5F'' and F'''). In contrast to this, cell clones expressing both EGFP-NLS and EGFP-Pt-Ets4 stopped dividing as soon they delaminated. In addition, when the cumulus started to migrate, the delaminated cells of the EGFP-

NLS/EGFP-Pt-Ets4 marked cell clone lost contact with each other and spread out underneath the germ-disc/germ-band epithelium (Video 3B, Figure 5G'' and G'''). This observation was consistent and reproducible in multiple analyzed embryos (Video 4).

These results demonstrate that *Ets4* expression is sufficient to induce cell delamination and migration in embryos of *P. tepidariorum*.

Ectopic expression of Pt-Ets4 induces mesoderm-like fate

As already mentioned, Pt-Ets4 seems to have no influence on the early expression of *Pt-dpp* itself (Figure 4A and E). Furthermore, we were not able to detect *Pt-dpp* transcripts in cells ectopically expressing Pt-Ets4 (Figure 6A and A'). In contrast to *Pt-dpp,* we did find that *Pt-Ets4* is regulating the expression of *Pt-hb.* While *Pt-hb* expression was nearly absent in *Pt-Ets4* RNAi embryos (Figure 4H), *Pt-hb* transcripts were present in the ectopically *Pt-Ets4* positive cell clone (Figure 6B and B').

The behavior of the Pt-Ets4 positive cells is reminiscent of migrating gastrulating cells that invade the germ-disc from the center and from the rim of the germ-disc [9, 20, 21] (see Video 1A). As Pt-Ets4 activates the expression of *Pt-hb* (a gene that is known to be expressed in mesodermal cells in diverse animals [22-24]) we wondered if *Pt-Ets4* misexpression is inducing a mesoderm-like cell fate. For this reason, we tested whether the ectopic expression of *Pt-Ets4* is also inducing the expression of the key mesodermal marker *Pt-twist* (*Pt-twi*). Indeed, *Pt-twi* was detectable within the cell clone that ectopically expressed Pt-Ets4 (Figure 6C and C', compare to controls in Figure 6—figure supplement 1). Interestingly, in the stage 4 embryos ectopically expressing Pt-Ets4, we could not only detect *Pt-twi* transcripts within the ectopic Pt-Ets4 expressing cell clone, but also within the central primary thickening (Figure 6C'). This comes as a surprise, as it was reported that *Pt-twi*

expression is not initiated before the end of stage 5 [21]. For this reason, we reanalyzed the full expression series of *Pt-twi* in wild-type embryos and we were able to confirm that *Pt-twi* is expressed in the developing primary thickening of stage 3 and 4 embryos (Figure 6—figure supplement 2A-C). Finally, we confirmed the regulation of *Pt-twi* via *Pt-Ets4* by analyzing the expression of *Pt-twi* in *Pt-Ets4* knockdown embryos. *Pt-twi* transcripts were no longer detectable in the primary thickening of stage 4 *Pt-Ets4* RNAi embryos (Figure 6D and E). However, late segmental mesoderm specification was unaffected as the expression of *Pt-twi* was unchanged in stage 7 *Pt-Ets4* knockdown embryos (Figure 6—figure supplement 2H-I'). This confirms that the formation and migration of the cumulus and later gastrulation events from central and peripheral parts of the germ-disc are two independent processes [8,14].

Overall, we suggest that the activation of *Pt-twi* and *Pt-hb* by Pt-Ets4 in cell clones initiated a mesoderm-like cell fate that led to the migratory behavior of the ectopic Pt-Ets4 positive cells.

Discussion

Ets proteins belong to a highly conserved family of transcription factors [25] that play a role in a variety of different cellular processes (e.g. growth, migration, differentiation) and it has been shown that these factors can act as activators or repressors of transcription [26-29]. In *D. melanogaster, Ets4* (also known as *Ets98B*) is expressed in the oocyte nucleus and the primordial germ cells (PGC) [30, 31] and there is evidence that *Dm-Ets4* is involved in the migration of the PGCs [32]. Furthermore, the mammalian homolog of *Ets4*, *Pdef,* is down regulated in invasive and migratory breast tumor cells [33]. Together, these reports suggest that Ets4 regulates migratory cell behavior in different organism.

Here we show that in the spider *P. tepidariorum, Ets4* is strongly expressed in the migrating cumulus and that *Pt-Ets4* is needed for the integrity of the cumulus, a group of cells, which need to migrate together in order to function normally. We also show that the ectopic expression of *Pt-Ets4* is able to ectopically induce cell delamination and cell migration within the ectodermal germ-disc cells (a process that is known as epithelial-to-mesenchymal transition [34, 35]). Taken together, these findings suggest that *Pt-Ets4* likely plays an important role in the migratory behavior of the cumulus.

It has been suggested that the cumulus cells of many higher spiders are specified during early embryogenesis and are not secondarily induced after the formation of the germ-disc [13]. *Pt-Ets4* marks the cells of the developing primary thickening (st. 3 and 4) and of the migrating cumulus. Therefore, our results indicate that also in *P. tepidariorum*, cumulus cells are induced before germ-disc formation is complete.

As the primary thickening forms in the absence of *Pt-Ets4*, *Pt-Ets4* cannot be the only factor that is required for the specification of the cells that will develop into the primary thickening (and later into the cumulus). This is supported by our finding that *Pt-Ets4* is sufficient to induce the delamination and migration of ectodermal cells, but it is not sufficient to induce the formation of a fully functional ectopic cumulus. So far, there have been no reports of any gene knockdown that completely inhibits the formation of the primary thickening. The cumulus is characterized by the co-expression of multiple genes, including *Pt-dpp*. As shown by our analyses, *Pt-Ets4* seems not to be involved in the regulation of *Pt-dpp* itself, as well as several other cumulus marker genes. Therefore, important factors of the cumulus are missing in the ectopic *Pt-Ets4* expression cells. Taken together, our findings indicate that the

311 formation of the primary thickening is a process that is buffered via the input of
312 several genes or other unknown mechanisms/factors.

313 Our results also show that an intact cumulus is needed to open up the germ-
314 disc and to initiate the formation of a bilaterally symmetric spider embryo. In the
315 germ-disc of *P. tepidariorum* embryos, BMP signaling is active from early stage 5
316 (Figure 3—figure supplement 1). However, the germ-disc does not open up before
317 the arrival of the cumulus at the rim of the disc at the end of stage 5 even though the
318 putative receptors are ubiquitously expressed. Therefore, the establishment of the
319 dorsal field is a precisely timed process, and it is possible that in *Pt-Ets4* knockdown
320 embryos the cells of the cumulus disperse too early, and are no longer able to induce
321 the opening of the germ-disc at the end of stage 5. An alternative, although not
322 mutually exclusive, explanation involves the fact that the cumulus may signal via
323 cytonemes [5,8]. These structures could be affected in *Pt-Ets4* RNAi embryos, as the
324 cumulus cells lose contact with each other. Lastly, *Pt-Ets4* could be involved in
325 regulating the BMP pathway activity at a different level (e.g. protein-protein
326 interactions, protein modifications) or the knockdown of *Pt-Ets4* could result in a fate
327 change of the cumulus cells before cumulus migration is initiated. Investigation of
328 each of these hypotheses will require the establishment of advanced techniques to
329 study cell migration, cell microstructure, and protein interactions in *P. tepidariorum*.

330 Via both our loss- and gain-of-function experiments, we found that *Pt-Ets4* is
331 involved in the activation of at least two genes that are expressed within the primary
332 thickening of stage 4 embryos. These genes are *Pt-hb* and *Pt-twi.* For *Pt-hb,* it was
333 already shown that this gene is strongly expressed within the primary thickening of
334 stage 4 embryos [22]. However, it was reported that *Pt-twi* expression is not
335 detectable before late stage 5 [21], while we found that *Pt-twi* is expressed in the
336 primary thickening already at stage 3 and 4. This is in agreement with our

337 sequencing data, which shows that *Pt-twi* is strongly up regulated from stage 2 to
338 stage 3 (Figure 1—figure supplement 1). This result indicates that the cumulus cells
339 are not endodermal in nature [4, 8, 14] but rather are mesendodermal. For this
340 reason, the genetic composition and the eventual fate of the cumulus should be
341 closely examined in future studies.
342
343 **Conclusions**
344 The cumulus is a fascinating example of a migrating and signaling organizer. Thus
345 far, cumulus-related dorsoventral patterning defects have been observed in spider
346 embryos that either completely lack BMP signaling or are deficient for cumulus
347 migration [6, 12]. Here, we show that the knockdown of the transcription factor *Pt-*
348 *Ets4* generates a novel dorsoventral phenotype that is dependent on cumulus
349 integrity. Our results show that formation of the bilaterally symmetric spider embryo is
350 a precisely timed process that relies on the presence of an intact, migrating and
351 signaling cumulus.
352
353 **Materials and Methods**
354 **Spider husbandry and embryology**
355 *Parasteatoda tepidariorum* adults and embryos were obtained from our laboratory
356 culture at the University of Cologne. Spiders were kept in plastic vials at room
357 temperature and fed with *Drosophila melanogaster* and crickets (*Acheta domesticus*
358 and *Gryllus bimaculatus*). Embryos were staged according to [9].
359
360 **Gene cloning**
361 PCR amplification and cloning of *Pt-Ets4* was performed using standard techniques.
362 *Pt-twist* (AB167807.1), *Pt-hunchback* (FM956092.1), *Pt-engrailed* (AB125741.1), *Pt-*

363 *fork-head* (AB096073.1), *Pt-armadillo* (AB120624.1), *Pt-orthodenticle* (AB096074.1),
364 *Pt-short-gastrulation* (AB236147.1), *Pt-decapentaplegic* (AB096072.1) and *Pt-fascin*
365 (AB433905.1) have been isolated previously.
366
367 **Identification and cloning of *Pt-Ets4* sequence**
368 The transcriptomes of the embryonic stages 1 - 3 (early stage 1, late stage 2 and
369 early stage 3; see Figure 1—figure supplement 1) were sequenced (HiSeq2000) at
370 the Cologne Center for Genomics. The total RNA of three cocoons per stage was
371 pooled and sequenced in each case.
372 The sequence reads (deposited to the Sequence Read Archive
373 (http://www.ncbi.nlm.nih.gov/sra/, BioProject ID: PRJNA383558) were mapped to the
374 AUGUSTUS gene predictions (https://i5k.nal.usda.gov/Parasteatoda_tepidariorum)
375 using Bowtie 2. New candidates were picked according to their expression profile.
376 These new candidates (including *Pt-Ets4;* AUGUSTUS prediction: *aug3.g4238*) were
377 up-regulated in a similar manner as *Pt-decapentaplegic*, *Pt-hedgehog* and *Pt-*
378 *patched* (genes that show a defect in dorsoventral patterning or cumulus migration
379 upon knockdown [6, 12] (see Figure 1—figure supplement 1). A 1094bp fragment of
380 *Pt-Ets4* was amplified using the primer Pt-g4238-Fw (5'-GTA CAC AGC ACC TTC
381 TAT TAT GG-3') and Pt-g4238-Rev (5'-CCT TCT TGT AAT ATT GGC GA-3') in an
382 initial PCR. For the production of dsRNA a T7 promoter sequence was added to the
383 5' and 3' end of the sequence by performing a nested PCR with the primer T7-Pt-
384 g4238-Fw (5'-GTA ATA CGA CTC ACT ATA GGG CCA CAA AAG ATG GCC-3') and
385 T7-Pt-g4238-Rev (5'-GTA ATA CGA CTC ACT ATA GGG GAA CGG CTG AGT
386 TTG-3'). This nested PCR yielded a 1046bp fragment that was used for the initial
387 knockdown of *Pt-Ets4*.
388

389 **RNAi**

390 Double stranded RNA (dsRNA) was produced using the MEGAscript T7 Kit
391 (ThermoFisher SCIENTIFIC).

392 Within one week, adult females of *Parasteatoda tepidariorum* were injected three to
393 four times with 2µl dsRNA solution (2-3µg/µl). Water injections served as a control.

394 The knockdown of *Pt-Ets4* was performed several times ($n_{experiments}$ >5; $n_{injected\ females}$
395 >24) and always resulted in the same phenotype. For the statistical analysis (Figure
396 2—figure supplement 1D-F) two non-overlapping fragments, targeting the CDS and
397 the 3'UTR of *Pt-Ets4,* were used (see Figure 2—figure supplement 1C). The coding
398 sequence of *Pt-Ets4* was amplified using the primer Pt-CDS-Ets4-Fw (5'-GTA GTC
399 TTG AAC TTC AGT TAT CAA AG-3') and Pt-CDS-Ets4-Rev (5'-GGT TTA CTT CAA
400 GAA CTG GAC-3') and was cloned into the pCR4 vector (ThermoFisher
401 SCIENTIFIC). The 3'UTR of *Pt-Ets4* was amplified using the primer Pt-3'Ets4-Fw (5'-
402 CAC TAT GGT TTC AAA CAT CGA TTG-3') and Pt-3'Ets4-Rev (5'-GTC ATA TCC
403 CCT CTA TAG CTA AC-3') and was cloned into the pCRII-Blunt vector
404 (ThermoFisher SCIENTIFIC). For the production of dsRNA the T7 promoter
405 sequence was added to both ends of the CDS and the 3'UTR fragment by using the
406 primer T7-Pt-CDS-Ets4-Fw (5'-GTA ATA CGA CTC ACT ATA GGG GTA GTC TTG
407 AAC TTC AGT TAT C-3') and T7-Pt-CDS-Ets4-Rev (5'-GTA ATA CGA CTC ACT
408 ATA GGG GTC TGA AGT AAT CTT CTG ATA G-3') and T7-Pt-3'Ets4-Fw (5'-GTA
409 ATA CGA CTC ACT ATA GGG CAC TAT GGT TTC AAA CAT CG-3') and T7-Pt-
410 3'Ets4-Rev (5'-GTA ATA CGA CTC ACT ATA GGG CCT AAA ACA CAG TTT TAG
411 GAG-3'), respectively. We observed a similar knockdown efficiency for both
412 fragments with the highest penetrance in the 3rd and 4th cocoons (Figure 2—figure
413 supplement 1E and F). As many embryos were able to recover from the knockdown
414 of *Pt-Ets4* during later stages of development (>stage 8, see Figure 2—figure

supplement 1G), the number of affected embryos was analyzed during the embryonic stages 6 and 7.

A gene fragment of *Pt-decapentaplegic* was amplified using the primers Pt-dpp-Fw (5'-GTG ATC ATA ACA GGT TCC TGA CC-3') and Pt-dpp-Rev (5'-GAC AAA GAA TCT TAA CGG CAA CC-3'). The resulting 1147bp *Pt-dpp* fragment was cloned into pCRII-Blunt vector. dsRNA template was generated by using T7 and T7Sp6 primer. The knockdown resulted in the same phenotype as published [6]. We used the *Pt-dpp* pRNAi embryos of a 4th cocoon (the development of 73 embryos of this cocoon were monitored under oil; 1 embryo died and 72 embryos showed a strong BMP signaling defect phenotype [6] during stages 6-8) to perform the *Pt-Ets4 in situ* staining shown in Figure 4—figure supplement 1A.

Two gene fragments of *Pt-patched* were amplified from a plasmid (containing a 2 kb fragment of *Pt-ptc*) using the primer T7-Pt-ptc-Fw1 (5'-GTA ATA CGA CTC ACT ATA GGG GGG TAG AAG ACG GCG G-3') and T7-Pt-ptc-Rev1 (5'-GTA ATA CGA CTC ACT ATA GGG GAG ACT CTT TAG CTA TAA TCT C-3') and T7-Pt-ptc-Fw2 (5'-GTA ATA CGA CTC ACT ATA GGG GAG ATT ATA GCT AAA GAG TCT C-3') and T7-Pt-ptc-Rev2 (5'-GTA ATA CGA CTC ACT ATA GGG GAT TTG TTT GTC GAC CAC C-3'). dsRNA of both fragments were combined and injected into adult *P. tepidariorum* females. The knockdown resulted in the same phenotype as published [12] (see right column in Figure 2, Video 1).

Phylogenetic analysis

Amino acid sequences were obtained from FlyBase [36], WormBase (WormBase release Version: WS257), or translated from the *P. tepidariorum* AUGUSTUS

441 predictions online (https://i5k.nal.usda.gov/Parasteatoda_tepidariorum). Amino acid
442 sequences were aligned using MUSCLE [37], alignments were trimmed using TrimAl
443 with the GappyOut setting [38], and maximum likelihood based phylogenies were
444 constructed using PhyML at “phylogeny.fr” [39]. Full amino acid sequences were
445 used for all genes except for *Pt-aug3.g5814.t1*, which is missing the N-terminus but
446 still contains the ETS domain (as predicted online [40]). Final phylogenies were
447 generated with the WAG substitution model and 1000 bootstrap replicates.
448 Phylogenetic analysis was also performed using the ETS domains alone, and while
449 tree topology changed in some ways, the *Ets-4* genes from *D. melanogaster* and *C.*
450 *elegans* still branched together with strong support, and the gene we have named *Pt-*
451 *Ets4* was the only *P. tepidariorum* gene branching together with this clade.
452
453 **Ectopic expression of Pt-Ets4 and EGFP**
454 Experiments have been performed by injecting capped mRNA into late stage 1
455 embryos of *P. tepidariorum*. Embryonic microinjections were performed as described
456 previously [15].
457 For the production of capped mRNA, the mMASSAGE mMACHINE Kit (T7 or Sp6,
458 ThermoFisher SCIENTIFIC) was used. Capped mRNA was injected at a
459 concentration of 2-3µg/µl.
460 For the ectopic expression of *Pt-Ets4* an EGFP-Pt-Ets4-PolyA fusion construct was
461 synthesized at Eurofins Genomics (see Figure 5—figure supplement 1; full sequence
462 available upon request). For the production of capped mRNA, the construct
463 contained a T7 and a Sp6 promoter at its 5’ end and could be linearized via NotI, PstI
464 or EcoRI restriction enzyme digest. In addition, the coding sequence of EGFP-Pt-
465 Ets4 was flanked by the 5’ and the 3’ UTR of the *Xenopus* beta-globin gene (also
466 used in *Tribolium* [41]). For the ectopic expression of NLS-EGFP, the *Pt-Ets4*

sequence of the EGFP-Pt-Ets4-PolyA construct was removed (via BglII, SalI double digest) and replaced by the sequence MAKIPPKKKRKVED (contains the SV40 T antigen nuclear localization signal [18]). For this, the primer BglII-NLS-SalI-Fw (5'-TTT AGATCT ATG GCT AAA ATT CCT CCC AAA AAG AAA CGT AAA GTT GAA GAT TAA GTCGAC TTT-3') and BglII-NLS-SalI-Rev (5'-AAA GTCGAC TTA ATC TTC AAC TTT ACG TTT CTT TTT GGG AGG AAT TTT AGC CAT AGATCT AAA-3') (coding for the NLS sequence) were annealed to each other, digested with BglII and SalI and inserted to the already cut vector. This resulted in an EGFP-NLS-PolyA construct (see Figure 5—figure supplement 1).

The function of *Pt-Ets4* was analyzed either by injecting capped mRNA of the Pt-Ets4-EGFP fusion construct alone or by injecting capped mRNA of *Pt-Ets4* (the EGFP was removed from the EGFP-Pt-Ets4-PolyA construct via an XhoI digest) together with capped mRNA of EGFP-NLS. Ectopic expression of *Pt-Ets4* co-injected with EGFP-NLS resulted in the same phenotype as shown for the EGFP-Pt-Ets4 fusion construct.

To obtain a stronger signal during live imaging, capped mRNA of EGFP-Pt-Ets4 was co-injected with EGFP-NLS.

To mark the membranes of the embryonic cells and to visualize the delamination process of the Pt-Ets4 positive cell clones, capped mRNA coding for lynGFP [19] was co-injected with capped mRNA coding for EGFP-Pt-Ets4. Next to the ectopic expression of lynGFP we tried to ectopically express GAP43YFP (another marker that was shown to localize to the cell membranes of *Tribolium* embryos [41, 42]). However, we observed a much stronger signal for lynGFP.

Whole mount *in situ* hybridization

Embryos were collected as described previously [5] with minor modifications. *In situ*

493 hybridization was performed as previously described [43] with minor modifications
494 (proteinase K treatment was not carried out). Fluorescent FastRed staining was
495 performed as described in [42].
496
497 *In situ* hybridization on *Pt-Ets4* RNAi embryos
498 RNAi embryos were fixed at the desired stage. The development of several embryos
499 of the same cocoon was monitored under oil. Only the embryos of severely affected
500 cocoons were used for this analysis. For each round of *in situ* hybridization (as a
501 control) the embryos from the same cocoons were analyzed for the expression of *Pt-*
502 *Ets4*.
503
504 Single embryo *in situ* hybridization
505 After the injection of capped mRNA coding for EGFP-Pt-Ets4, pictures of the single
506 living embryos that exhibited an EGFP-Pt-Ets4 positive cell clone were taken. The
507 same embryos were fixed by injecting 10% formaldehyde to the perivitelline space
508 and were incubated for several hours at room temperature. To remove the oil, the
509 single embryos were transferred to heptane and the chorion was removed using
510 forceps. Subsequently, the single embryos were transferred to 100% methanol and
511 the vitelline membrane was removed using forceps. *In situ* hybridization on the single
512 embryos was performed as described above.
513
514 **pMAD antibody staining**
515 To analyze BMP pathway activity in control and *Pt-Ets4* knockdown embryos a
516 pMAD antibody staining was performed in embryos that were already stained for *Pt-*
517 *otd* (via *in situ* hybridization). Embryos were fixed as usual (see above).
518 *In situ* stained embryos were washed in PBST (3 x 15 min) and blocked in PBST

519 containing 0,1% BSA and 5% goat serum (1 hour at RT). Subsequently, the embryos
520 were transferred to a fresh solution of PBST containing 0,1% BSA and 5% goat
521 serum. The Phospho-Smad1/5 (Ser463/465) (41D10) Rabbit mAb (Cell Signaling
522 Technology, Inc.) was added to this solution (antibody concentration: 1:1000; 4°C
523 o.n.). On the next day the embryos were washed in PBST (3 x15 min) and were
524 blocked again in PBST containing 0,1% BSA and 5% goat serum (1 hour at RT). The
525 secondary antibody (Anti-Rabbit IgG, couplet to alkaline phosphatase (AP), produced
526 in goat; A3687 SIGMA) was added to the blocking solution at a 1:1000 concentration.
527 After incubating the secondary antibody for 2-3 hours (RT) excessive antibody was
528 removed by washing the embryos several times in PBST (6 x 15 min; final washing
529 step at 4°C o.n.). Finally, a regular NBT/BCIP staining was carried out (see whole
530 mount *in situ* hybridization).
531
532 **EGFP antibody staining**
533 We used an anti green fluorescent protein mouse IgG antibody (A11120;
534 ThermoFischer SCIENTIFIC; final concentration 1:1000) as primary and an Alexa
535 Fluor 488 goat anti mouse IgG (A11001; ThermoFischer SCIENTIFIC; final
536 concentration 1:400) as secondary antibody.
537
538 **Durcupan sections**
539 To stain all of the embryonic cells, *in situ* hybridization with the ubiquitously
540 expressed gene *Pt-arm* was carried out in early stage 5 embryos of control and *Pt-*
541 *Ets4* RNAi embryos. Embryos were then stained with Sytox Green (1:5000 in PBST,
542 ThermoFischer SCIENTIFIC). Embryos were then gradually (50%, 70%, 90%)
543 transferred to 100% EtOH. After a washing step in 1:1 EtOH/acetone, the embryos
544 were transferred to 100% acetone. Single embryos were transferred to microtome

545 embedding molds in a 1:1 durcupan/acetone solution. Acetone was removed by
546 incubating the embryos at room temperature (o.n.). The embedding molds were filled
547 with fresh durcupan (Fluka). Polymerisation of the durcupan was carried out at 65°C
548 (16-20 hours). Cross sectioning (8µm) was performed on a LEICA RM 2255
549 microtome.
550
551 **Bioinformatics**
552 RNA from stage 1-3 embryos was extracted and sequenced as described in the
553 "Identification of *Pt-Ets4*" section above. These sequences were made available for
554 us to download from the Cologne Centre for Genomics server, and FastQC [44] was
555 used for initial assessment of read quality. This was excellent (lower quartile Phred
556 quality above 30 until the last base in the read, no residual adapter sequence noted)
557 and as such no trimming was performed. Comparative expression analysis was
558 performed by mapping reads to *Parasteatoda_tepidariorum* AUGUSTUS gene
559 predictions (https://i5k.nal.usda.gov/Parasteatoda_tepidariorum) using RSEM 1.2.28
560 [45] and Bowtie 1.0.0 [46] as packaged in the Trinity 2.2.0 module (-est_method
561 RSEM—aln_method bowtie [47]). Cross sample normalization was performed using
562 Trimmed Mean of M-values, and edgeR [48] was run to determine differential
563 expression with a dispersion ratio fixed at 0.1. Those differentially expressed genes
564 with a p-value cut off for FDR of 0.001 and min abs(log2(a/b)) change of 2 were then
565 chosen for annotation and further examination, with target gene results provided in
566 Figure 1—figure supplement 1.
567
568 **Imaging and image processing**
569 Pictures were taken using an Axio Zoom.V16 that was equipped with an AxioCam
570 506 color camera. Confocal imaging was performed on a LSM 700 (Zeiss). Live

imaging was carried out on the Axio Zoom.V16, a Zeiss AxioImager.Z2 (equipped with an AxioCam MRm camera and a movable stage) and on a Leica CLSM SP8 (Imaging facility Biocenter Cologne).

Projections of image stacks were carried out using Helicon Focus (HeliconSoft) or Fiji [49].

All movies have been recorded at room temperature and images have been adjusted for brightness and contrast using Adobe Photoshop CS5.

For false-color overlays of *in situ* hybridization images a bright field image of the NBT/BCIP staining was inverted. This inverted picture was pasted into the red channel of the nuclear stain image. The input levels (Adobe Photoshop CS5; Levels function) of the red channel were adjusted in a way that only the signal of the NBT/BCIP staining remained visible.

Author contributions

M.P. conceived the project. M.P., S.R. and M.A.B. designed the experiments. M.P. and M.A.B. performed the experiments. M.A.B. performed the phylogenetic analysis. N.J.K. and N.P. performed the bioinformatic analyses. M.P., M.A.B. and S.R. interpreted the results. M.P. wrote the initial draft of the paper. All authors contributed to the writing of the final manuscript. All authors approved the final manuscript.

Acknowledgments

We thank Evelyn Schwager for details on the durcupan-sectioning protocol and Mette Handberg-Thorsager for providing the lynEGFP construct. We thank Hiroki Oda and Maarten Hilbrant for comments on the manuscript.

Funding

M.P. was supported by the Deutsche Forschungsgemeinschaft (DFG; grant numbers PE 2075/1-1 and PE 2075/1-2).

M.A.B. was supported by a Humboldt Fellowship for Postdoctoral Researchers.

N.P. was supported by a grant of the Volkswagen Foundation (project number: 85 983) and by the Emmy Noether program of the Deutsche Forschungsgemeinschaft (grant number: PO 1648/3-1).

The funders had no role in study design, data collection and interpretation, or the decision to submit the work for publication.

Competing financial interests

The authors declare no competing financial interests.

References

1. Spemann H, Mangold H. Induction of embryonic primordia by implantation of organizers from a different species. 1923. Int J Dev Biol. 2001;45(1):13–38.
2. De Robertis EM. Spemann's organizer and the self-regulation of embryonic fields. Mech Dev. Dezember 2009;126(11–12):925–41.
3. Anderson C, Stern CD. Chapter Twenty-Six - Organizers in Development. In: Wassarman PM,. Current Topics in Developmental Biology. Academic Press; 2016. S. 435–54. (Essays on Developmental Biology, Part B; Bd. 117). http://www.sciencedirect.com/science/article/pii/S0070215315001891
4. Oda H, Akiyama-Oda Y. Differing strategies for forming the arthropod body plan: lessons from Dpp, Sog and Delta in the fly Drosophila and spider Achaearanea. Dev Growth Differ. Mai 2008;50(4):203–14.

623 5. Akiyama-Oda Y, Oda H. Early patterning of the spider embryo: a cluster of
624 mesenchymal cells at the cumulus produces Dpp signals received by germ
625 disc epithelial cells. Development. 1. Mai 2003;130(9):1735–47.
626 6. Akiyama-Oda Y, Oda H. Axis specification in the spider embryo: dpp is
627 required for radial-to-axial symmetry transformation and sog for ventral
628 patterning. Development. 15. Juni 2006;133(12):2347–57.
629 7. McGregor AP, Hilbrant M, Pechmann M, Schwager EE, Prpic N-M, Damen
630 WGM. Cupiennius salei and Achaearanea tepidariorum: Spider models for
631 investigating evolution and development. Bioessays. Mai 2008;30(5):487–98.
632 8. Hilbrant M, Damen WGM, McGregor AP. Evolutionary crossroads in
633 developmental biology: the spider Parasteatoda tepidariorum. Development. 1.
634 August 2012;139(15):2655–62.
635 9. Mittmann B, Wolff C. Embryonic development and staging of the cobweb
636 spider Parasteatoda tepidariorum C. L. Koch, 1841 (syn.: Achaearanea
637 tepidariorum; Araneomorphae; Theridiidae). Dev Genes Evol. Juli
638 2012;222(4):189–216.
639 10. Schwager EE, Schönauer A, Leite DJ, Sharma PP, McGregor AP. Chelicerata.
640 In: Wanninger A, Herausgeber. Evolutionary Developmental Biology of
641 Invertebrates 3. Springer Vienna; 2015. S. 99–139.
642 http://link.springer.com/chapter/10.1007/978-3-7091-1865-8_5
643 11. Holm Å. Experimentelle Untersuchungen über die Entwicklung und
644 Entwicklungsphysiologie des Spinnenembryos. Zool. BiDr Uppsala (1952) 29,
645 293-424.
646

12. Akiyama-Oda Y, Oda H. Cell migration that orients the dorsoventral axis is coordinated with anteroposterior patterning mediated by Hedgehog signaling in the early spider embryo. Development. 15. April 2010;137(8):1263–73.

13. Edgar A, Bates C, Larkin K, Black S. Gastrulation occurs in multiple phases at two distinct sites in Latrodectus and Cheiracanthium spiders. EvoDevo. 2015;6:33.

14. Oda H, Nishimura O, Hirao Y, Tarui H, Agata K, Akiyama-Oda Y. Progressive activation of Delta-Notch signaling from around the blastopore is required to set up a functional caudal lobe in the spider Achaearanea tepidariorum. Development. Juni 2007;134(12):2195–205.

15. Pechmann M. Formation of the germ-disc in spider embryos by a condensation-like mechanism. Front Zool. 2016;13:35.

16. Pechmann M, McGregor AP, Schwager EE, Feitosa NM, Damen WGM. Dynamic gene expression is required for anterior regionalization in a spider. Proc Natl Acad Sci USA. 3. Februar 2009;106(5):1468–72.

17. Akiyama-Oda Y, Oda H. Multi-color FISH facilitates analysis of cell-type diversification and developmental gene regulation in the Parasteatoda spider embryo. Develop Growth Differ. 1. Februar 2016;58(2):215–24.

18. Kanayama M, Akiyama-Oda Y, Oda H. Early embryonic development in the spider Achaearanea tepidariorum: Microinjection verifies that cellularization is complete before the blastoderm stage. Arthropod Structure & Development. November 2010;39(6):436–45.

19. Köster RW, Fraser SE. Tracing transgene expression in living zebrafish embryos. Dev Biol. 15. Mai 2001;233(2):329–46.

20. Kanayama M, Akiyama-Oda Y, Nishimura O, Tarui H, Agata K, Oda H. Travelling and splitting of a wave of hedgehog expression involved in spider-head segmentation. Nat Commun. 11. Oktober 2011;2:500.

21. Yamazaki K, Akiyama-Oda Y, Oda H. Expression patterns of a twist-related gene in embryos of the spider Achaearanea tepidariorum reveal divergent aspects of mesoderm development in the fly and spider. Zool Sci. Februar 2005;22(2):177–85.

22. Schwager EE, Pechmann M, Feitosa NM, McGregor AP, Damen WGM. hunchback functions as a segmentation gene in the spider Achaearanea tepidariorum. Curr Biol. 25. August 2009;19(16):1333–40.

23. Franke FA, Mayer G. Expression study of the hunchback ortholog in embryos of the onychophoran Euperipatoides rowelli. Dev Genes Evol. 1. Juli 2015;225(4):207–19.

24. Kerner P, Zelada González F, Le Gouar M, Ledent V, Arendt D, Vervoort M. The expression of a hunchback ortholog in the polychaete annelid Platynereis dumerilii suggests an ancestral role in mesoderm development and neurogenesis. Dev Genes Evol. Dezember 2006;216(12):821–8.

25. Laudet V, Hänni C, Stéhelin D, Duterque-Coquillaud M. Molecular phylogeny of the ETS gene family. Oncogene. 11. Februar 1999;18(6):1351–9.

26. Oikawa T, Yamada T. Molecular biology of the Ets family of transcription factors. Gene. 16. Januar 2003;303:11–34.

27. Sharrocks AD, Brown AL, Ling Y, Yates PR. The ETS-domain transcription factor family. Int J Biochem Cell Biol. Dezember 1997;29(12):1371–87.

28. Sharrocks AD. The ETS-domain transcription factor family. Nat Rev Mol Cell Biol. November 2001;2(11):827–37.

29. Hollenhorst PC, McIntosh LP, Graves BJ. Genomic and biochemical insights into the specificity of ETS transcription factors. Annu Rev Biochem. 2011;80:437–71.

30. Chen T, Bunting M, Karim FD, Thummel CS. Isolation and characterization of five Drosophila genes that encode an ets-related DNA binding domain. Developmental Biology. 1. Mai 1992;151(1):176–91.

31. Hsouna A, Watson DK, Hsu T. Developmental expression pattern of D-ets4, the Drosophila homologue of human Pdef. Gene Expr Patterns. Dezember 2004;5(2):285–9.

32. Hsouna A, Ivey J, Hsu T. The role of D-Ets-4 in germ cell migration during Drosophila embryonic development. (2003) A. Dros. Res. Conf. 44 : 554B. (FlyBase ID: FBrf0154875).

33. Feldman RJ, Sementchenko VI, Gayed M, Fraig MM, Watson DK. Pdef Expression in Human Breast Cancer Is Correlated with Invasive Potential and Altered Gene Expression. Cancer Res. 1. August 2003;63(15):4626–31.

34. Thiery JP, Acloque H, Huang RYJ, Nieto MA. Epithelial-mesenchymal transitions in development and disease. Cell. 25. November 2009;139(5):871–90.

35. Gilmour D, Rembold M, Leptin M. From morphogen to morphogenesis and back. Nature. 19. Januar 2017;541(7637):311–20.

36. dos Santos G, Schroeder AJ, Goodman JL, Strelets VB, Crosby MA, Thurmond J, u. a. FlyBase: introduction of the Drosophila melanogaster Release 6 reference genome assembly and large-scale migration of genome annotations. Nucleic Acids Res. Januar 2015;43(Database issue):D690-697.

37. Edgar RC. MUSCLE: multiple sequence alignment with high accuracy and high throughput. Nucleic Acids Res. 2004;32(5):1792–7.

722 38. Capella-Gutiérrez S, Silla-Martínez JM, Gabaldón T. trimAl: a tool for
723 automated alignment trimming in large-scale phylogenetic analyses.
724 Bioinformatics. 1. August 2009;25(15):1972–3.
725 39. Dereeper A, Guignon V, Blanc G, Audic S, Buffet S, Chevenet F, u. a.
726 Phylogeny.fr: robust phylogenetic analysis for the non-specialist. Nucleic Acids
727 Res. 1. Juli 2008;36(Web Server issue):W465-469.
728 40. de Castro E, Sigrist CJA, Gattiker A, Bulliard V, Langendijk-Genevaux PS,
729 Gasteiger E, u. a. ScanProsite: detection of PROSITE signature matches and
730 ProRule-associated functional and structural residues in proteins. Nucleic
731 Acids Res. 1. Juli 2006;34(Web Server issue):W362–5.
732 41. Benton MA, Akam M, Pavlopoulos A. Cell and tissue dynamics during
733 Tribolium embryogenesis revealed by versatile fluorescence labeling
734 approaches. Development. August 2013;140(15):3210–20.
735 42. Benton MA, Pechmann M, Frey N, Stappert D, Conrads KH, Chen Y-T, u. a.
736 Toll Genes Have an Ancestral Role in Axis Elongation. Curr Biol. 20. Juni
737 2016;26(12):1609–15.
738 43. Prpic N-M, Schoppmeier M, Damen WGM. Whole-Mount In Situ Hybridization
739 of Spider Embryos. Cold Spring Harb Protoc. 10. Januar
740 2008;2008(10):pdb.prot5068.
741 44. Andrews S. FastQC: A quality control tool for high throughput sequence data
742 [Website]. 2010. http://www.bioinformatics.babraham.ac.uk/projects/fastqc/
743 45. Li B, Dewey CN. RSEM: accurate transcript quantification from RNA-Seq data
744 with or without a reference genome. BMC Bioinformatics. 2011;12:323.
745 46. Langmead B. Aligning short sequencing reads with Bowtie. Curr Protoc
746 Bioinformatics. Dezember 2010;Chapter 11:Unit 11.7.

47. Grabherr, M.G., et al. Full-length transcriptome assembly from RNA-Seq data without a reference genome. Nat Biotechnol. United States 29: 644–652 (2011).

48. Robinson MD, McCarthy DJ, Smyth GK. edgeR: a Bioconductor package for differential expression analysis of digital gene expression data. Bioinformatics. 1. Januar 2010;26(1):139–40.

49. Schindelin J, Arganda-Carreras I, Frise E, Kaynig V, Longair M, Pietzsch T, u. a. Fiji: an open-source platform for biological-image analysis. Nat Methods. 28. Juni 2012;9(7):676–82.

Figures

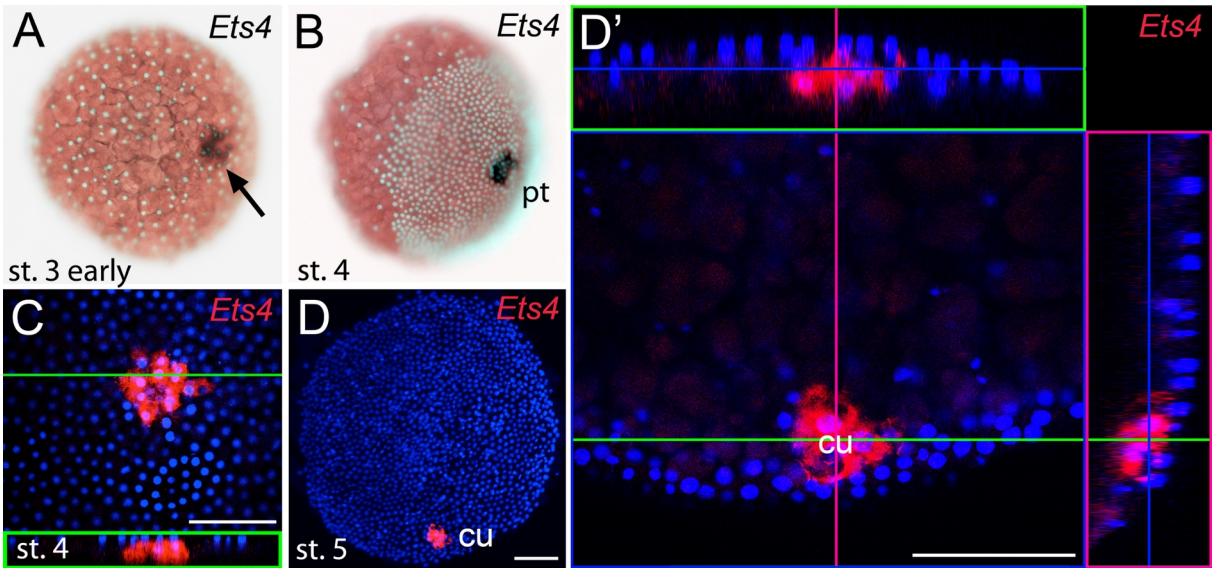

Figure 1. Early embryonic expression of *Pt-Ets4*. (A and B) *Pt-Ets4* is expressed within the cluster of cells (arrow in A) that will develop into the central primary thickening (pt) (B). (C-D') Confocal scans (single optical slices (C and D'); maximum intensity projection (D)) of embryos stained for *Pt-Ets4* (FastRed stain; red) and nuclei (DAPI; blue). *Pt-Ets4* is expressed within the primary thickening and in the migrating cumulus (cu), which are covered by the surface epithelium of the germ-disc. Orthogonal views are boxed in green and magenta. The same embryo is depicted in D and D'. Scale bar is 100µm.

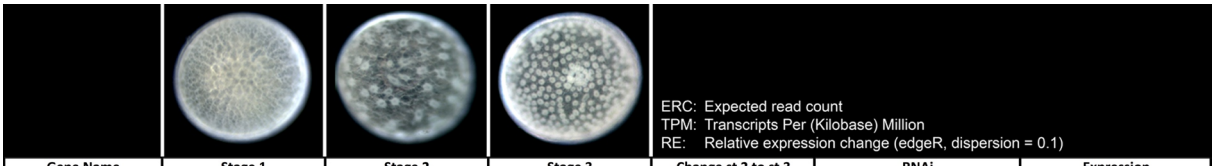

Gene Name (AUGUSTUS Prediction)	Stage 1		Stage 2		Stage 3		Change st 2 to st 3		RNAi phenotype	Expression stage 3
	ERC	TPM	ERC	TPM	ERC	TPM	RE	FDR		
Pt-hedgehog (aug3.g4322.t1)	5	0.184	136	5.712	1674	67.195	10.08	1.54E-04	cumulus migration defect (Akiyama-Oda and Oda 2010)	extra-embryonic cells (Akiyama-Oda and Oda 2010)
Pt-patched (aug3.g14374.t2)	107.18	1.082	344.54	4.015	3438.37	38.241	8.16	5.32E-04	cumulus migration defect (Akiyama-Oda and Oda 2010)	primary thickening (Akiyama-Oda and Oda 2010)
Pt-decapentaplegic (aug3.g16926.t1)	48	0.572	47	0.648	272	3.564	4.73	1.96E-02	ventralized (Akiyama-Oda and Oda 2010)	not detectable via in situ hybridisation
Pt-Ets4 (aug3.g4238.t1)	4	0.092	155	3.914	1930	46.572	10.20	1.36E-04	ventralized/cumulus integrity (this work)	primary thickening (this work)
Pt-twist (aug3.g14287.t1)	0	0	36	1.889	526	26.464	11.93	8.28E-05	unpublished	primary thickening (this work)

766

767 **Figure 1—figure supplement 1. Expression profile analysis.** Expression profile in
768 embryonic stages 1-3, RNAi phenotypes and expression of the genes *Pt-hh*, *Pt-ptc*,
769 *Pt-dpp*, *Pt-Ets4* and *Pt-twi*.

770

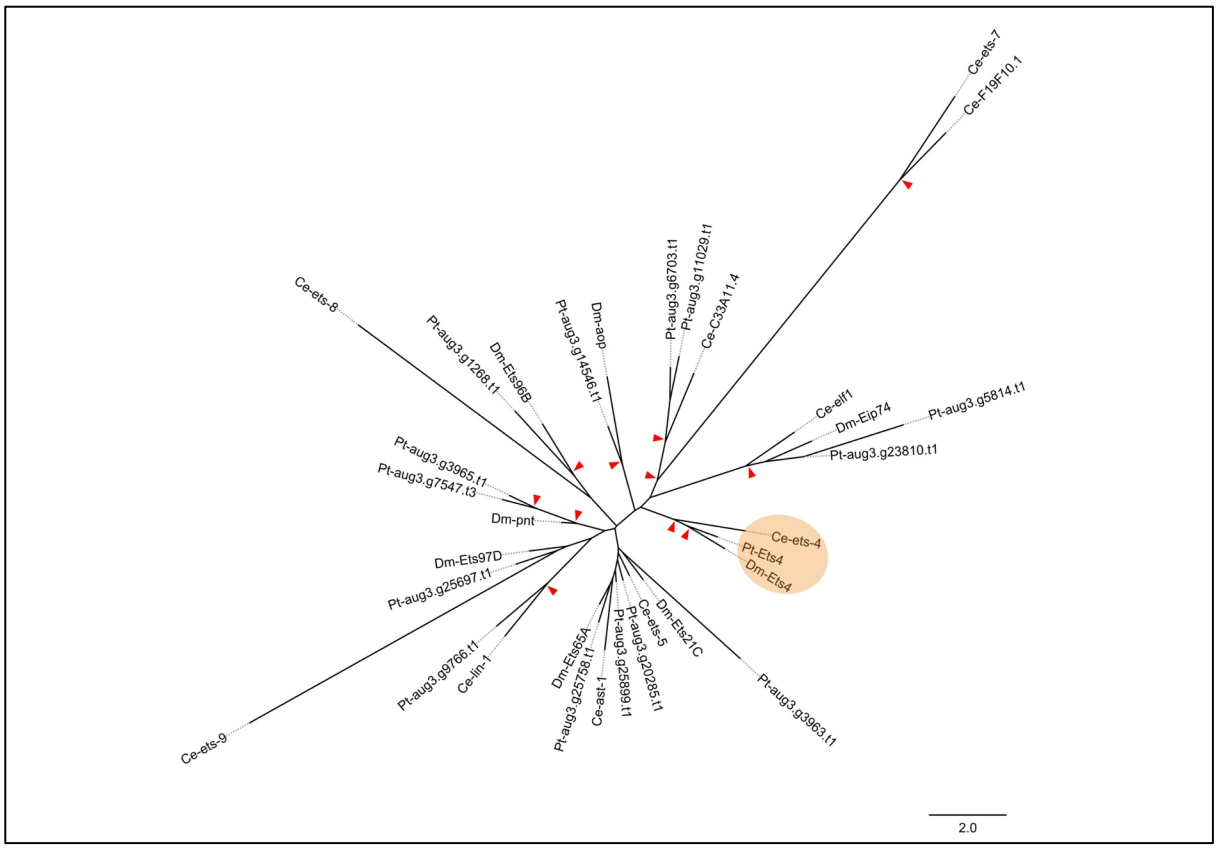

771

772 **Figure 1—figure supplement 2. Phylogenetic analysis.** Maximum likelihood
773 phylogeny of all ETS-family genes from *D. melanogaster* (Dm), *C. elegans* (Ce) and
774 *P. tepidariorum* (Pt). Red arrowheads mark nodes with bootstrap support greater
775 than 80. Scale is substitutions per site.

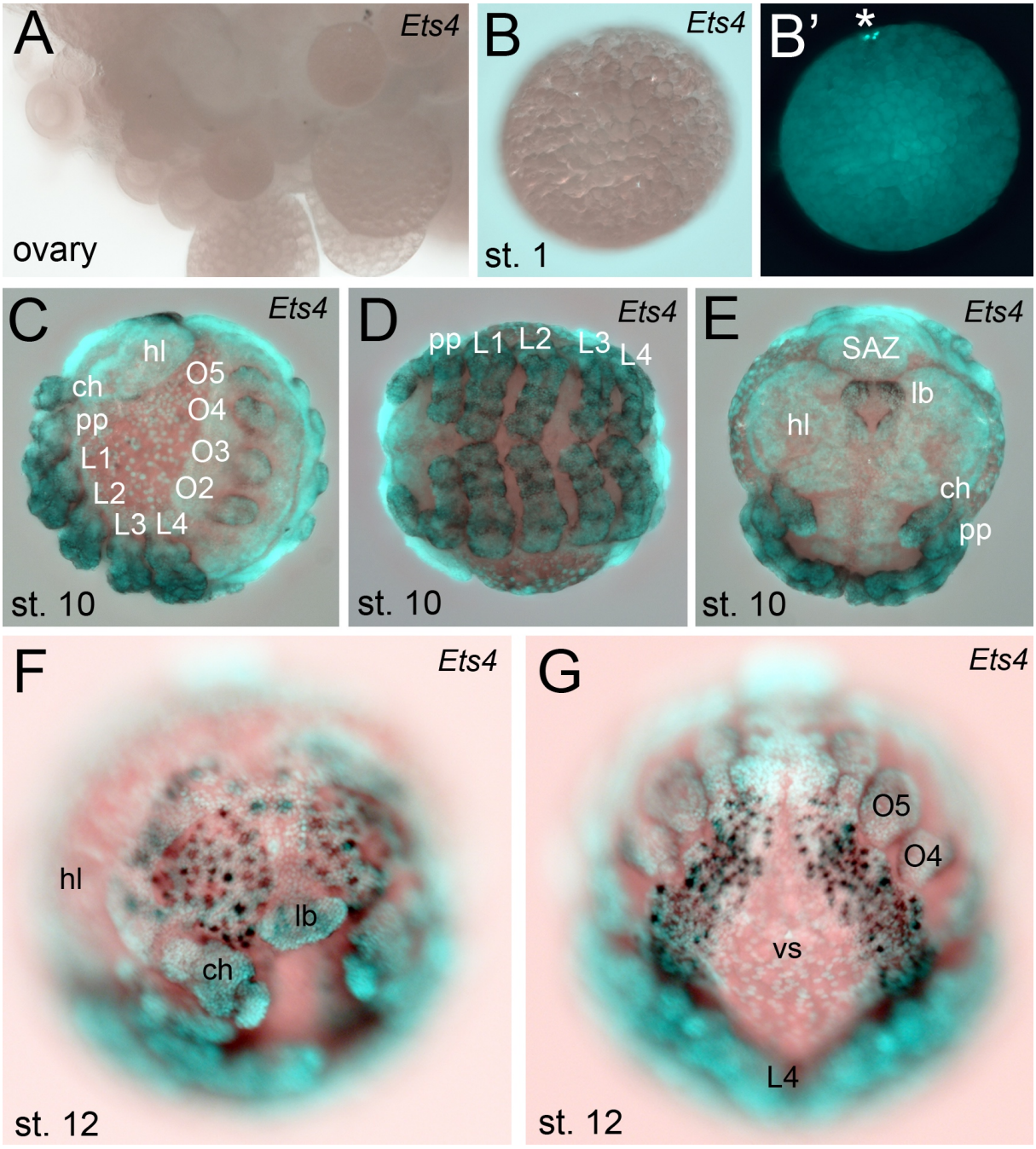

776

777 **Figure 1—figure supplement 3. Extended expression analysis of *Pt-Ets4*.** *Pt-*

778 *Ets4* is not expressed in ovaries (A) and early stage 1 embryos (B and B'). Asterisk in

779 B' marks the polar bodies. (C-E) Expression of *Pt-Ets4* at stage 10 (lateral view (C),

780 ventral view (D), anterior view (E)). *Pt-Ets4* is expressed in all developing

781 appendages of the prosoma (ch-L4) and of the opisthosoma (O2-O5). Within the

782 prosomal appendages *Pt-Ets4* is expressed in rings (D). *Pt-Ets4* is strongly

783 expressed within the labrum (E) and in lateral domains surrounding the stomodeum.

784 (F and G) Additional expression of *Pt-Ets4* in the nervous system is detectable at
785 embryonic stage 12 (anterior view (F); ventral view on the anterior part of the
786 opisthosoma (G)). Abbreviations: ch: chelicera; pp: pedipalpus; L1-L4: walking legs
787 1-4, O2-O5: opisthosomal limb buds 2-5 (O2 develops into the book lung, O3
788 develops into trachea, O4 and O5 develop into the spinnerets); hl: head lobes; lb:
789 labrum; vs: ventral sulcus; SAZ: segment addition zone.
790

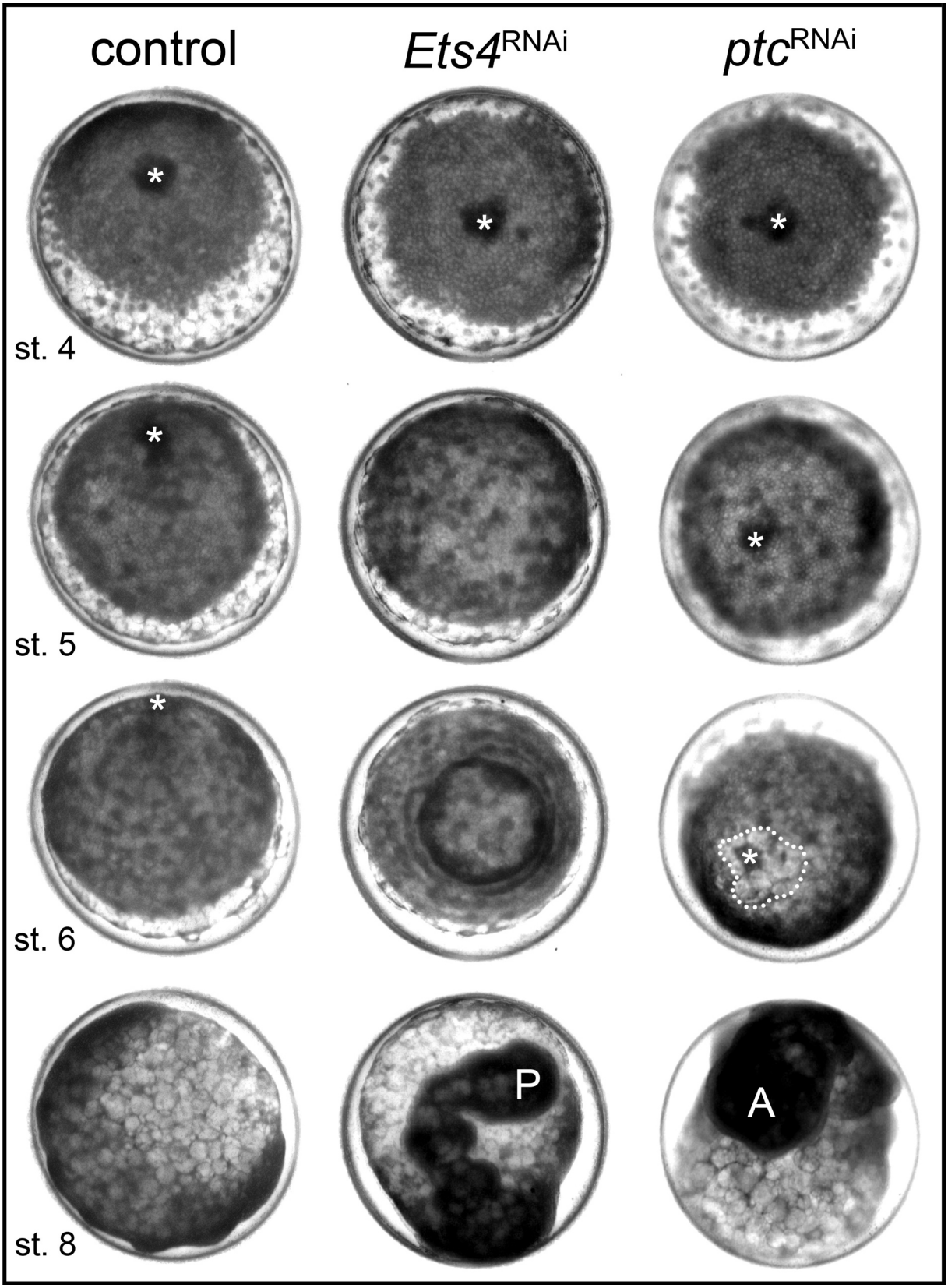

Figure 2. *Pt-Ets4* is required for cumulus integrity.

Stills from the embryos shown in Video1. The cumulus (asterisk) migrates in the control, disappears in the *Pt-Ets4* RNAi and stays in the center of the germ-disc in *Pt-*

ptc RNAi embryo. Ectopic, central opening (induction of the dorsal field) of the germ-disc is depicted via the dotted line (*Pt-ptc* RNAi st. 6). Posterior (P) and anterior (A) tube formation in *Pt-Ets4* and *Pt-ptc* knockdown embryos is also indicated.

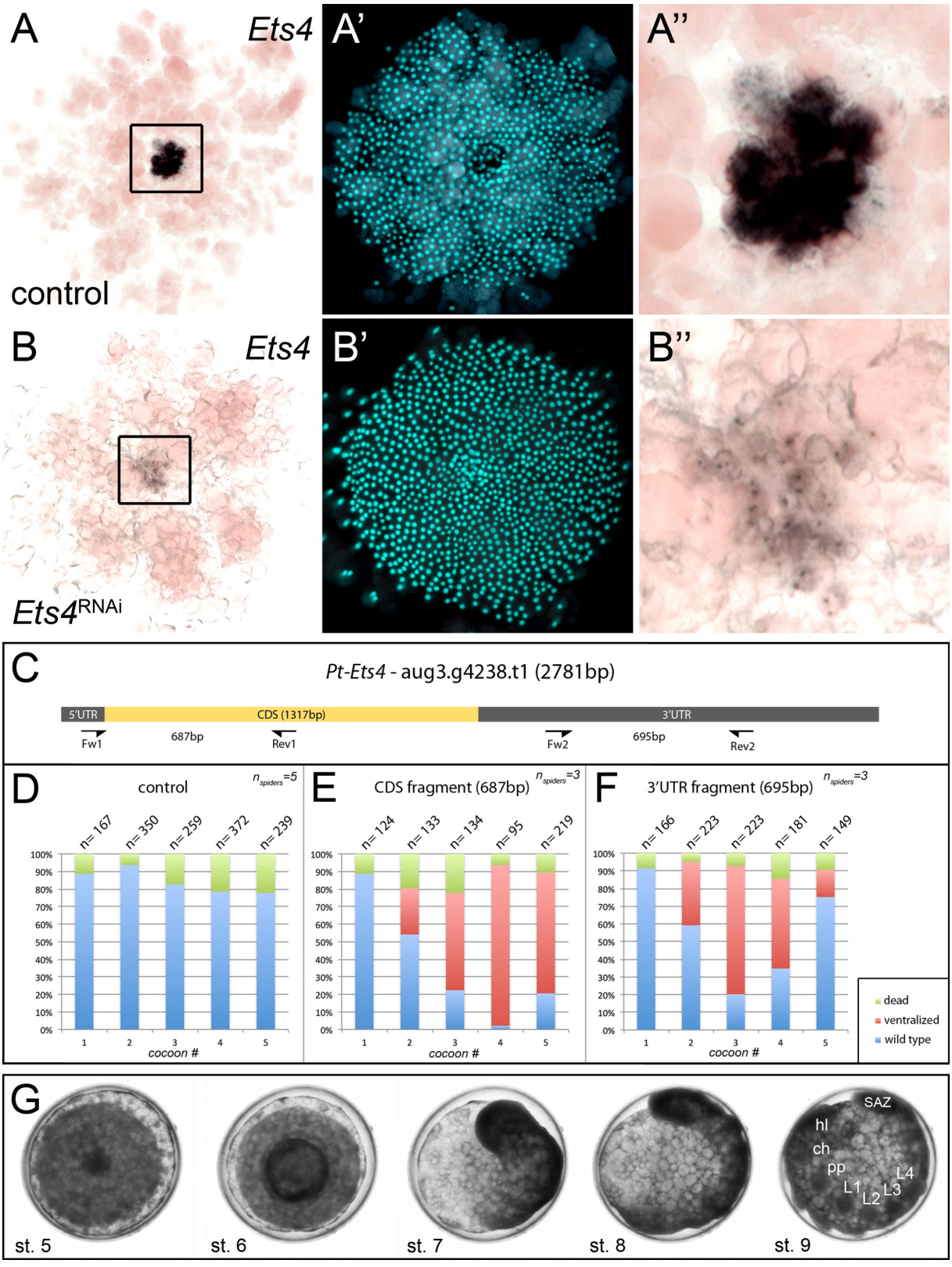

Figure 2—figure supplement 1. Knockdown efficiency after RNAi with *Pt-Ets4*. In comparison to the control embryo (A-A'') the expression of *Pt-Ets4* is strongly silenced after *Pt-Ets4* RNAi (B-B''). Nascent *Pt-Ets4* transcripts are still detectable in the nuclei of the primary thickening. The boxed region in A and B is magnified in A'' and B''. (C) Schematic representation of the AUGUSTUS prediction for *Pt*-Ets4 including the location of the untranslated regions (5' and 3' UTR), the coding sequence (CDS) and the primers (T7-Pt-CDS-Ets4-Fw (Fw1), T7-Pt-CDS-Ets4-Rev (Rev1), T7-Pt-3'Ets4-Fw (Fw2), T7-Pt-3'Ets4-Rev (Rev2), see Material and Methods) that were used to generate two non-overlapping fragments of *Pt-Ets4* that were used in the RNAi experiments (see Material and Methods). (D-F) Statistical analysis of the knockdown efficiency after pRNAi with the CDS fragment and the 3'UTR fragment of *Pt-Ets4*. As many embryos were able to completely recover from the *Pt-Ets4* knockdown at later stages of development (see embryo shown in G) the embryos were analyzed for their phenotypes at embryonic stages 6 and 7. (G) Stills from a time-lapse imaging experiment showing a strongly affected *Pt-Ets4* RNAi embryo at developmental stages 6 and 7. The tube-like structure elongates from the posterior, folds back onto the yolk and re-establishes a DV axis during stages 8 and 9. The embryo has fully recovered from the early DV phenotype at stage 9 of development. This demonstrates the regulatory capacities of spider embryos.

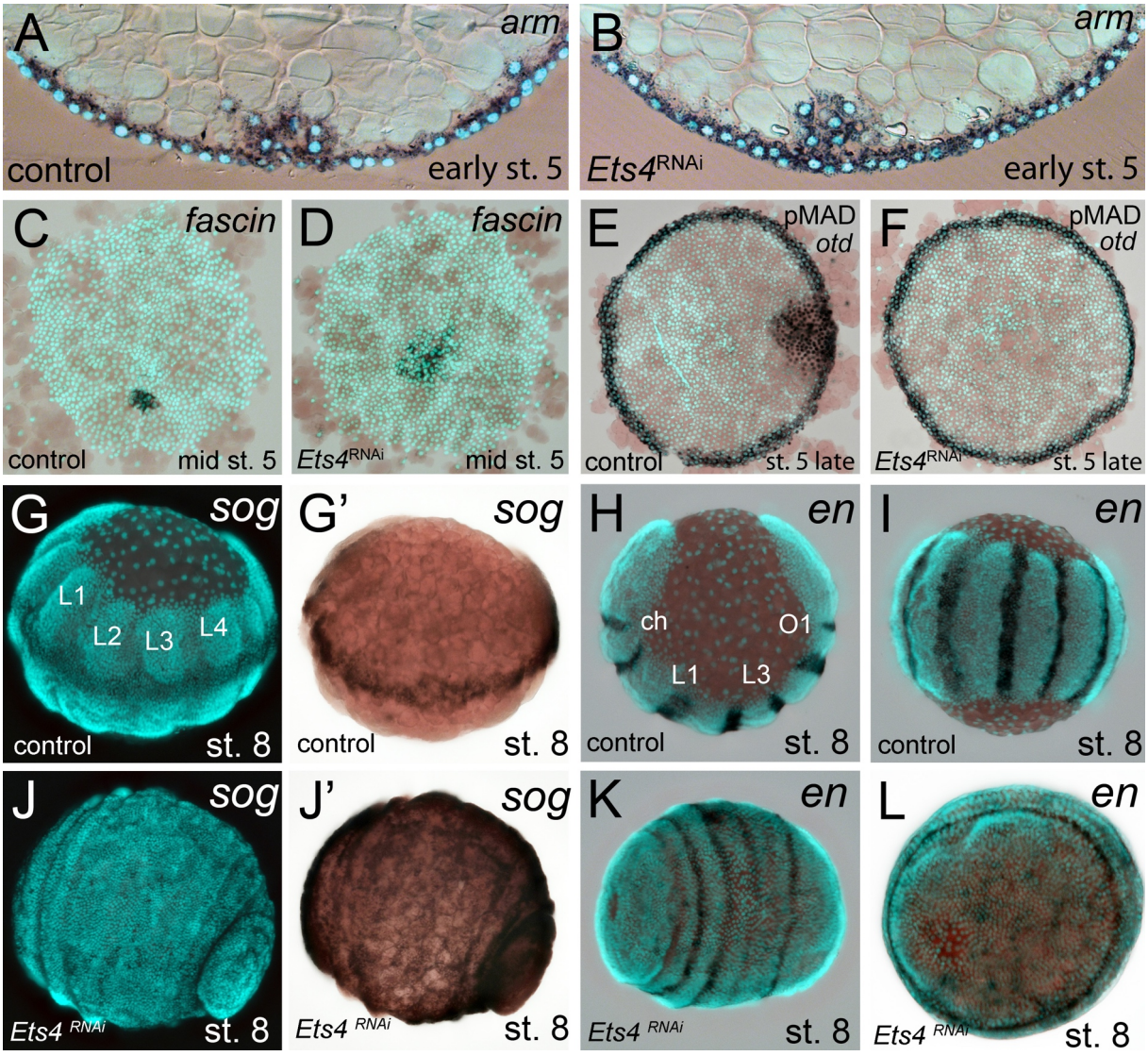

Figure 3. Cumulus integrity and signaling is affected in *Pt-Ets4* knockdown embryos.

(A and B) Cross-section through the central cumulus of ubiquitously stained (via *Pt-arm* RNA *in situ* hybridization) control (A) and *Pt-Ets4* RNAi (B) embryos. (C and D) control and *Pt-Ets4* RNAi embryos stained for the cumulus marker *Pt-fascin.* Cells of the cumulus are dispersing in the *Pt-Ets4* knockdown embryo (D). (E and F) Single color double stain of anterior *Pt-otd* expression (anterior ring) and nuclear localized pMAD in the cells overlaying the cumulus. pMAD signal is absent in *Pt-Ets4* RNAi embryos (F). *In situ* hybridization for the ventral fate marker *Pt-sog* (G, G', J and J') or the segmental marker *Pt-en* (H, I, K and L) in control (G-I) and *Pt-Ets4* knockdown

embryos (J-L). The same embryos in fluorescence vs. bright field channel are shown in G and G' as well as in J and J'. Nuclear stain (DAPI)/bright field overlay is shown in A-F, H, I, K and L. Flat mounted embryos in C-F. Lateral-ventral view (G, G', J-K), lateral view (H), ventral view (I). Abbreviations: ch: cheliceral segment; L1-L4: walking leg bearing segments 1-4; O1: opisthosomal segment 1.

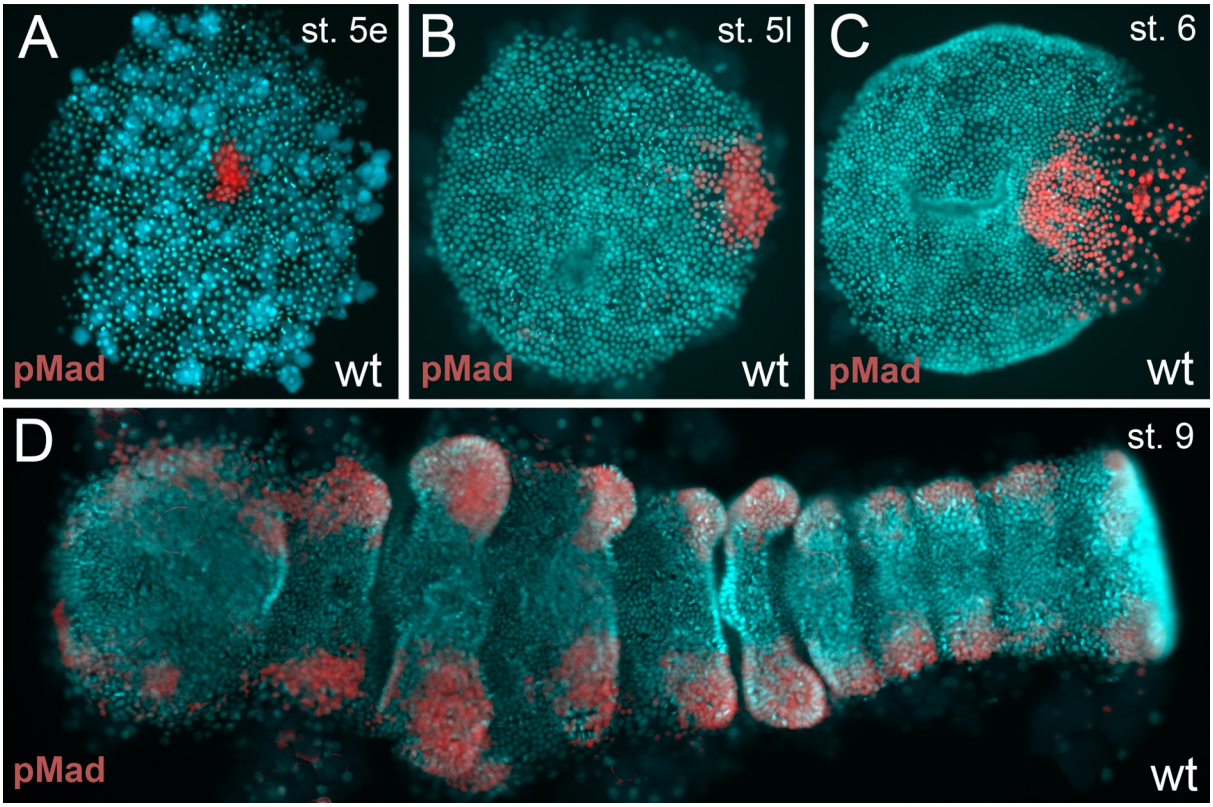

Figure 3—figure supplement 1. BMP pathway activity in wt embryos. (A-D) The BMP signaling pathway (visualized via pMad antibody staining; false color images) is active from early stage 5 onwards. However, the germ-disc does not open up before late stage 5, after the cumulus has reached the rim of the disc.

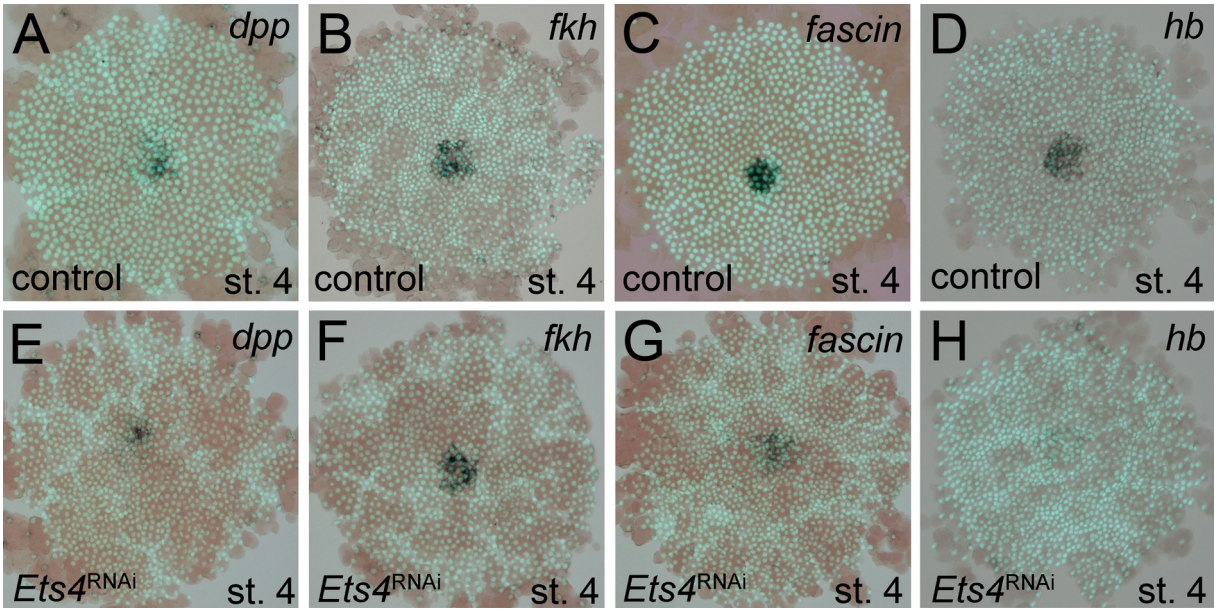

Figure 4. Analysis of "cumulus marker" genes. Flat mount preparation of *in situ* stained stage 4 embryos. While *Pt-dpp* and *Pt-fkh* expression is unaffected (compare A to E and B to F), *Pt-fascin* expression is slightly (compare C to G) and *Pt-hb* expression is strongly down regulated in *Pt-Ets4* RNAi embryos (compare D to H).

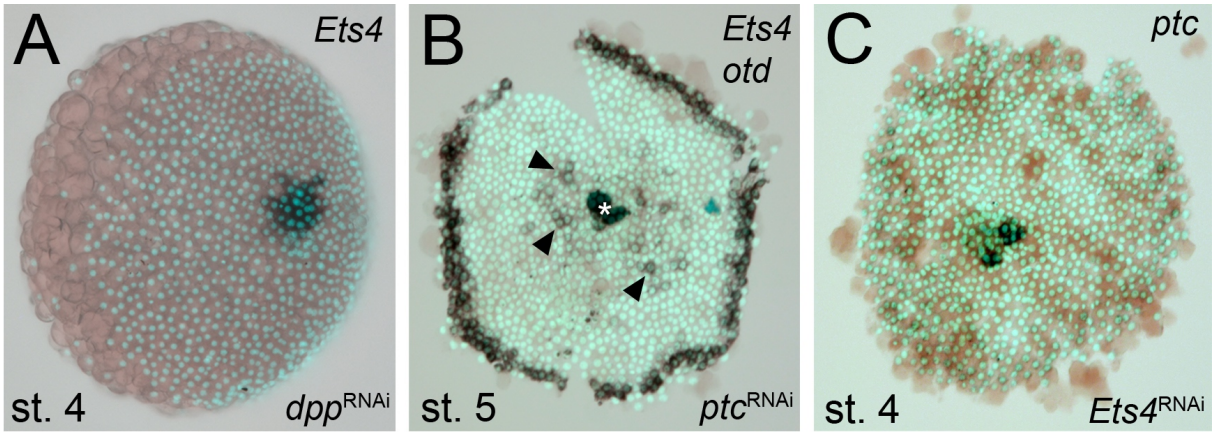

Figure 4—figure supplement 1. Regulation of *Pt-Ets4* and *Pt-ptc*. (A) *Pt-dpp* does not regulate the expression of *Pt-Ets4*. (B) Single color double staining detecting cumulus-specific *Pt-Ets4* and anterior *Pt-otd* transcripts in a *Pt-ptc* RNAi embryo. Strong *Pt-Ets4* expression (asterisk) is detectable in a *Pt-ptc* RNAi embryo. As already described [12], *Pt-otd* is ectopically activated in the center of the germ-disc (arrowheads). (C) Pt-Ets4 does not regulate the expression of *Pt-ptc*.

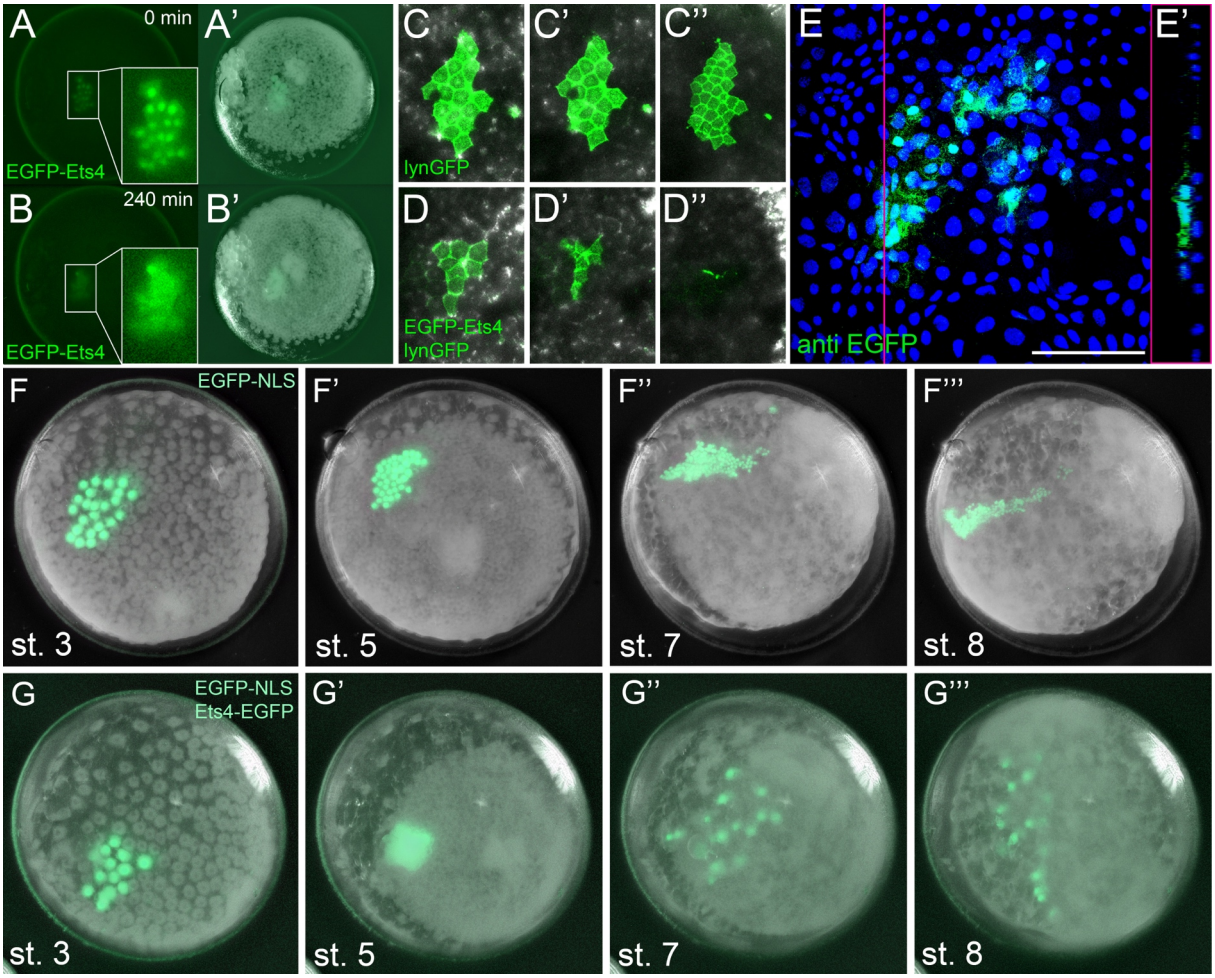

Figure 5. Ectopic expression of *Pt-Ets4* causes the delamination and migration of cells.

(A and A') A stage 4 embryo in which a cell clone has been marked via the ectopic expression of an EGFP-Pt-Ets4 fusion construct. The fusion protein localizes to the nuclei. (B and B') The cell clone has delaminated four hours later. As the overlaying epithelium is highly light-scattering, the nuclear EGFP signal is no longer visible. The inset shows the magnification of the boxed region in A and B. (C and D) Stills from Video 2A and 2D (magnifications of the lynGFP positive regions). Cells expressing lynGFP alone (C-C'') stay at the surface epithelium of the germ-disc. Cells expressing lynGFP/EGFP-Pt-Ets4 (D-D'') constrict and delaminate. (E) EGFP antibody staining (maximum intensity projection is shown in E and the orthogonal

868 view is shown in E') of a fixed embryo ectopically expressing EGFP-Pt-Ets4. (F-F''')
869 Stills from Video 3A (control). A cell clone marked via the ectopic expression of
870 nuclear localized EGFP (EGFP-NLS) marks the ectoderm during germ-band
871 formation. (G-G''') Stills from Video 3B (ectopic expression of *Pt-Ets4*). A cell clone
872 ectopically expressing EGFP-Pt-Ets4 in combination with EGFP-NLS delaminates
873 after germ-disc formation (G'). The cells of this cell clone start to disperse during later
874 stages of development (G'' and G'''). Scale bar is 100µm in E.
875

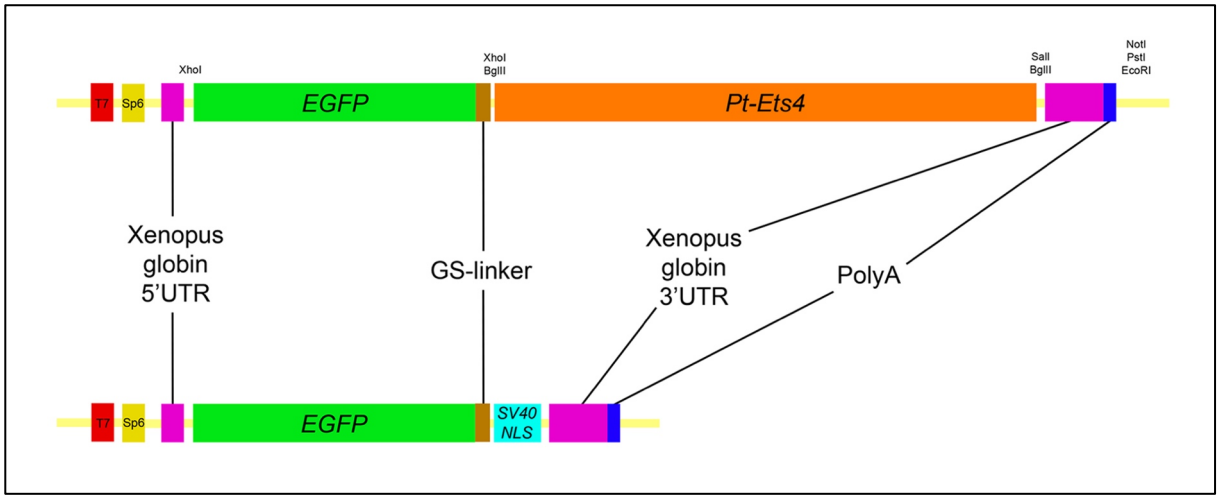

876

877 **Figure 5—figure supplement 1. Constructs.** Schematic representation of the
878 constructs that were used for the production of capped mRNA. The EGFP-Pt-Ets4
879 fusion construct was synthesized and cloned into the pUC57 vector by Eurofins
880 Genomics. This construct was modified (see Material and Methods) to generate the
881 nuclear localized form of EGFP (via insertion of the SV40-NLS sequence). Location
882 of used restriction sites (used for modification and linearization) is indicated above
883 the EGFP-Pt-Ets4 fusion construct. The PolyA tail consists of 25 residues.
884

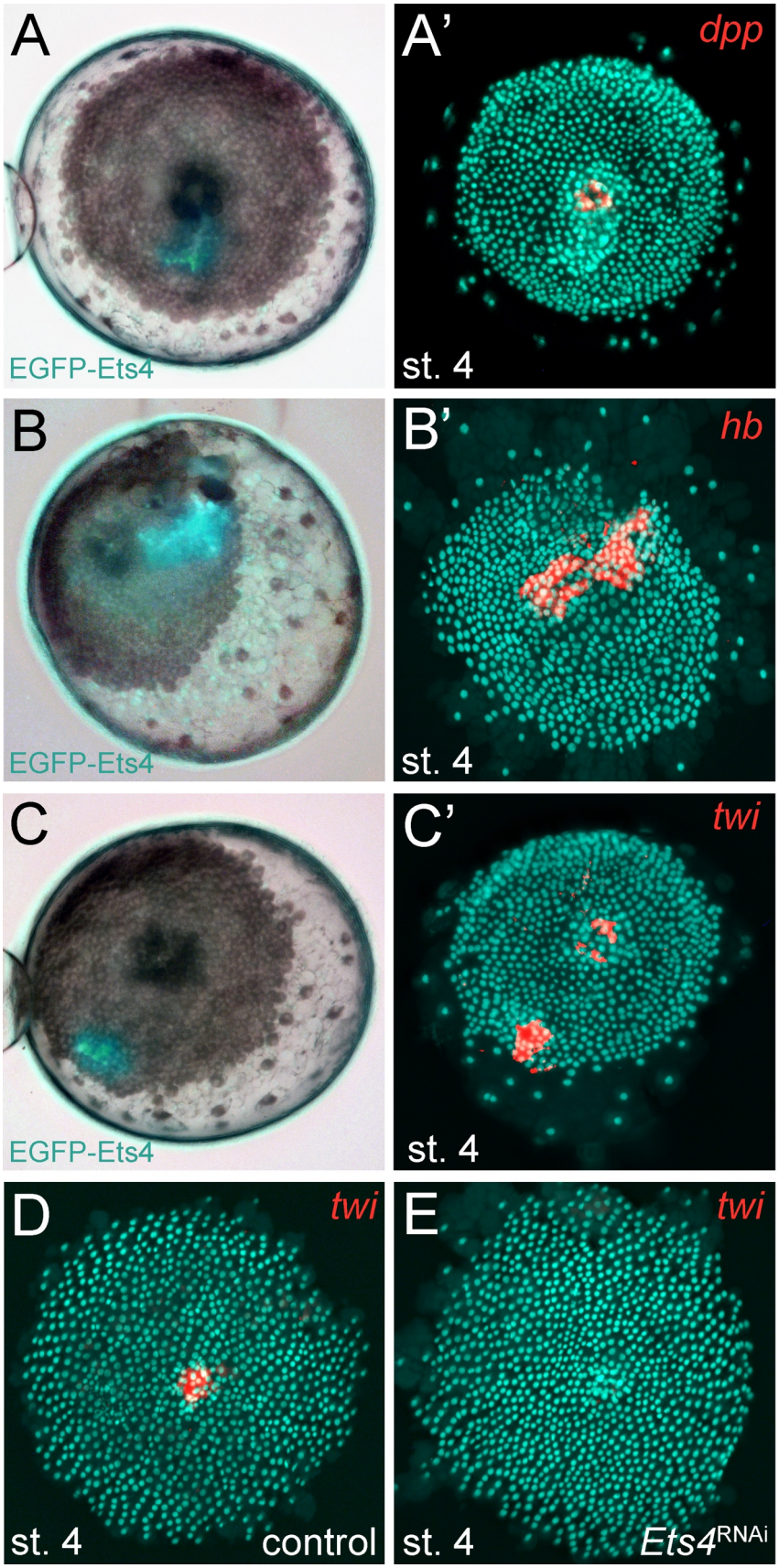

Figure 6. *Pt-Ets4* regulates *Pt-hb* and *Pt-twi* expression within the primary thickening.

888 Live stage 4 embryos in which a cell clone is marked via the ectopic-expression of
889 EGFP-Ets4 are depicted in A-C. The same embryos have been fixed and analyzed
890 for their expression of *Pt-dpp* (A'), *Pt-hb* (B') and *Pt-twi* (C'), respectively. Expression
891 of *Pt-twi* in a control (D) and a *Pt-Ets4* knockdown embryo (E). A', B', C', D and E are
892 false-color overlays of *in situ* hybridization images.
893

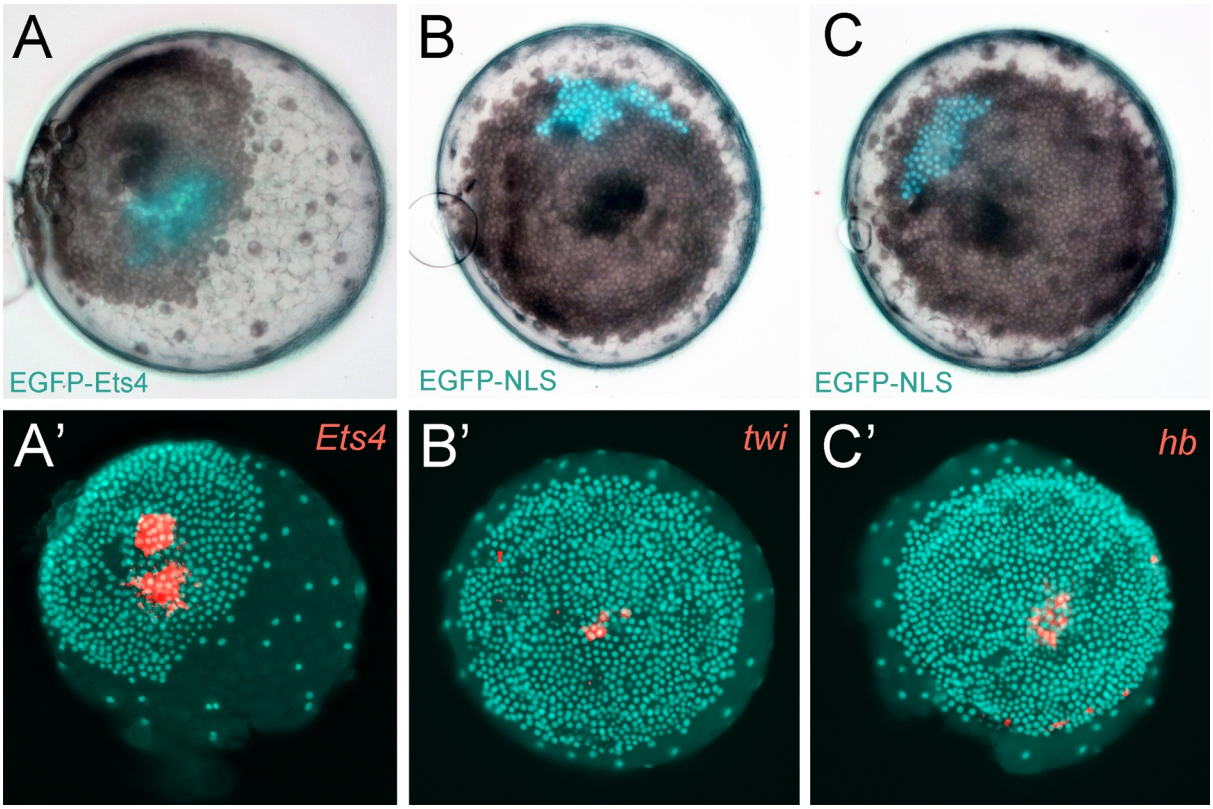

894

895 **Figure 6—figure supplement 1. Controls for the ectopic expression of EGFP-**
896 **Ets4.** (A-C) Live stage 4 control embryos in which a cell clone is marked via the
897 ectopic expression of EGFP-Ets4 (A) or EGFP-NLS (B and C). The same embryos
898 have been fixed and analyzed for their expression of *Pt-Ets4* (A'), *Pt-twi* (B') and *Pt-*
899 *hb* (C'), respectively (false-color overlays of *in situ* hybridization images). Injected
900 *EGFP-Ets4* mRNA is detectable within the marked cell clone (A'). The cell clones
901 ectopically expressing EGFP-NLS are negative for *Pt-twi* and *Pt-hb* transcripts (B'
902 and C').

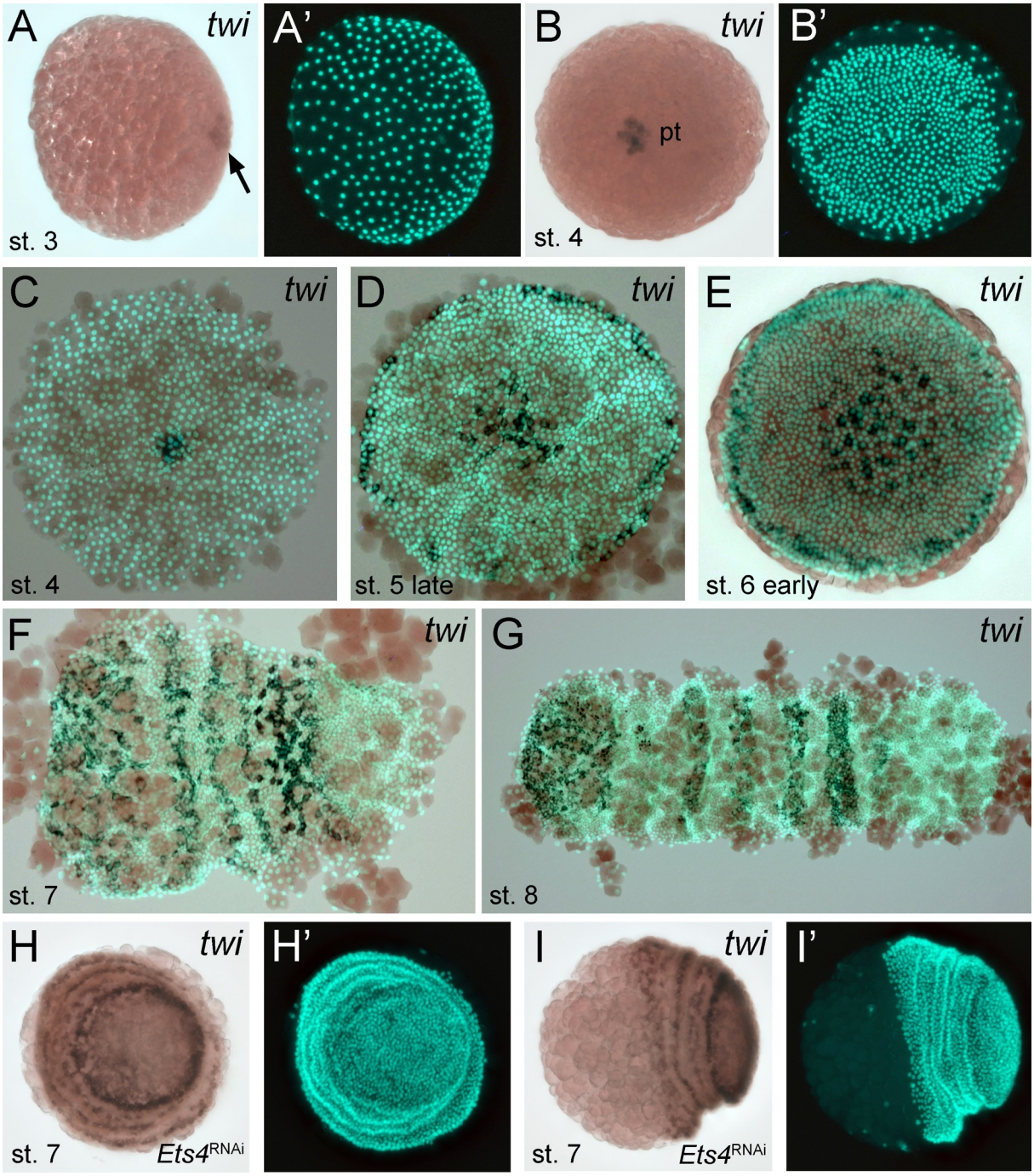

903

904 **Figure 6—figure supplement 2. Expression of *Pt-twi* in wt and *Pt-Ets4* RNAi**
905 **embryos.** Newly discovered expression of *Pt-twi* in the central cell cluster of the
906 forming germ-disc (arrow in A) and the primary thickening (pt in B) is depicted in (A-
907 C). The already published expression of *Pt-twist* [21] is depicted in (D-G). The
908 expression of *Pt-twi* in stage 7 *Pt-Ets4* RNAi embryos is not affected (H and I).
909 Anterior is to the left (where possible).

910

911 **Video 1. Knockdown of *Pt-Ets4* and *Pt-ptc*.** Live imaging of a control (A), a *Pt-Ets4*
912 RNAi (B) and a *Pt-ptc* RNAi (C) embryo under transmitted light conditions. The video
913 starts at stage 3 and ends at stage 9 of embryonic development. Cumulus migration
914 and normal germ-band formation is visible in the control embryo (A). The cells of the
915 cumulus disperse in the *Pt-Ets4* knockdown embryo (B). The ventralized *Pt-Ets4*
916 RNAi embryo stays radially symmetric and posterior tube formation is initiated (30h
917 onwards). The cumulus of the *Pt-ptc* RNAi embryo does not migrate (C). The germ-
918 disc opens up at the central position and the radially symmetric embryo overgrows
919 the yolk and anterior tube formation is initiated (48h onwards).
920
921 **Video 2. Ectopic expression of Pt-Ets4 causes the delamination of cells.** Ectopic
922 expression of lynGFP (A) and lynGFP in combination with EGFP-Ets4 (B-D). The
923 lynGFP positive cell clone (A) stays in the ectodermal cell layer of the germ-disc.
924 Regardless of the shape of the cell clones, Pt-Ets4 positive cells apically constrict
925 and delaminate (B-D).
926
927 **Video 3. Ectopic expression of Pt-Ets4 causes the delamination and migration**
928 **of cells.** Ectopic expression of EGFP-NLS (A) and EGFP-NLS in combination with
929 EGFP-Ets4 (B). The cell clone positive for EGFP-NLS (A) stays in the ectodermal cell
930 layer of the germ-disc. Cells further divide and form a long and thin cell clone (via
931 convergent extension [20]) at stage 8 of embryonic development. The Pt-Ets4
932 positive cell clone delaminates at stage 4 (B). Cells stop dividing and start to disperse
933 as soon as the cells of the cumulus start to migrate (st. 5).
934
935 **Video 4. Ectopic expression of EGFP-NLS and EGFP-Pt-Ets4 in multiple**
936 **embryos.** Ectopic expression of EGFP-NLS (A-D) and EGFP-NLS in combination

937 with EGFP-Ets4 (E-H). EGFP-NLS (A-D) and ectopic clones expressing Pt-Ets4 (E-
938 H) have equal positions within the germ-disc. While all of the control cell clones (A-D)
939 form long and thin stretched cell clones at stage 8 of embryonic development, the Pt-
940 Ets4 positive cells clones (E-H) delaminate and the cells disperse from stage 5
941 onwards. Only the EGFP channel is shown for all embryos.